

PERSPECTIVE | JULY 24 2024

Extracellular vesicle and lipoprotein diagnostics (ExoLP-Dx) with membrane sensor: A robust microfluidic platform to overcome heterogeneity

Sonu Kumar  ; Satyajyoti Senapati  ; Hsueh-Chia Chang  

 Check for updates

Biomicrofluidics 18, 041301 (2024)

<https://doi.org/10.1063/5.0218986>



Articles You May Be Interested In

Challenges and opportunities in exosome research—Perspectives from biology, engineering, and cancer therapy

APL Bioeng. (March 2019)

Vascularized platforms for investigating cell communication via extracellular vesicles

Biomicrofluidics (September 2024)

A novel viscoelastic microfluidic platform for nanoparticle/small extracellular vesicle separation through viscosity gradient-induced migration

Biomicrofluidics (June 2024)

Extracellular vesicle and lipoprotein diagnostics (ExoLP-Dx) with membrane sensor: A robust microfluidic platform to overcome heterogeneity

Cite as: Biomicrofluidics 18, 041301 (2024); doi: 10.1063/5.0218986

Submitted: 14 May 2024 · Accepted: 4 July 2024 ·

Published Online: 24 July 2024



View Online



Export Citation



CrossMark

Sonu Kumar, Satyajyoti Senapati, and Hsueh-Chia Chang^{a)}

AFFILIATIONS

Department of Chemical and Biomolecular Engineering, University of Notre Dame, Notre Dame, Indiana 46556, USA

^{a)}Author to whom correspondence should be addressed: hchang@nd.edu

ABSTRACT

The physiological origins and functions of extracellular vesicles (EVs) and lipoproteins (LPs) propel advancements in precision medicine by offering non-invasive diagnostic and therapeutic prospects for cancers, cardiovascular, and neurodegenerative diseases. However, EV/LP diagnostics (ExoLP-Dx) face considerable challenges. Their intrinsic heterogeneity, spanning biogenesis pathways, surface protein composition, and concentration metrics complicate traditional diagnostic approaches. Commonly used methods such as nanoparticle tracking analysis, enzyme-linked immunosorbent assay, and nuclear magnetic resonance do not provide any information about their proteomic subfractions, including active proteins/enzymes involved in essential pathways/functions. Size constraints limit the efficacy of flow cytometry for small EVs and LPs, while ultracentrifugation isolation is hampered by co-elution with non-target entities. In this perspective, we propose a charge-based electrokinetic membrane sensor, with silica nanoparticle reporters providing salient features, that can overcome the interference, long incubation time, sensitivity, and normalization issues of ExoLP-Dx from raw plasma without needing sample pretreatment/isolation. A universal EV/LP standard curve is obtained despite their heterogeneities.

26 May 2025 19:54:44

Published under an exclusive license by AIP Publishing. <https://doi.org/10.1063/5.0218986>

I. INTRODUCTION

Extracellular vesicles (EVs) represent a heterogeneous group of biomolecular assemblies, all characterized by a distinctive lipid bilayer and hydrophilic core, instrumental in a myriad of biological processes.^{1–7} This umbrella term includes exosomes, which are 30–150 nm in size and originate from endosomal biogenesis, and microvesicles, ranging from 100 to 1000 nm and emerging through the outward budding of plasma membranes.^{1–9} Each plays a unique, pivotal role in mediating intercellular communication, inducing immune responses,^{14–17} and participating in various pathological processes.^{18–23} Conversely, lipoproteins (LPs), characterized by a lipid monolayer surrounding a hydrophobic core, are categorized into several broad subtypes: High-Density Lipoprotein^{24–28} (HDL, 5–12 nm), Low-Density Lipoprotein^{29–31} (LDL, 18–28 nm), and Very Low-Density Lipoprotein^{32–35} (VLDL, 30–80 nm). There is a new class of recently discovered extracellular amembranous nanoparticles in a similar size range—exosomes (30–50 nm)³⁶ and supermeres (15–25 nm).³⁷ As both are amembranous in nature, they are classified as neither LPs nor EVs.

The biological systems capitalize on the distinct hydrophobic and hydrophilic cores depending on the nature of the cargo.^{4,7–9,24,38–41} The contrasting hydrophilic and hydrophobic cores of EVs and LPs, respectively, facilitate the transit of both hydrophobic^{24–31,33,42–44} and hydrophilic^{8,9,38} molecules to target destinations, securely isolating their cargo to prevent the undesired interactions during transport while ensuring that the cargo remains in functional and active states.⁴⁵ For instance, several proteins and nucleic acids, susceptible to degradation in the extracellular matrix (ECM), are safely housed within the hydrophilic core of EVs, maintaining their functionality.^{46–51} Matrix Metalloproteinases (MMPs) secreted by metastatic tumor cells remodel the extracellular matrix (ECM) to enable invasion and proliferation and may inform the metastatic status of cancers⁵² and can be on EVs from several biological sources.^{39–41,53,54} In contrast, hydrophobic molecules find their place in the core of LPs, facilitating their transport to and from the liver.^{24–26,29–31,33} Additionally, EVs also carry transmembrane and surface proteins they inherit from the cell or organelle membranes, including the signature tetraspanins (CD63, CD9,

CD81)—the protein composition of their membranes typically mirrors that of their originating cells and the molecular processes through which they are formed.^{55,56} This means that EVs carry unique signatures from their source cells, including distinct disease biomarkers, an overabundance of non-coding RNAs, and proteins related to specific disease pathways, notably those proteins central to prevalent cancer pathways, such as KRAS,^{57–61} PI3K,^{62–64} and p53.⁶⁵ Moreover, proteins are considered to be more reliable biomarkers and the predictor of a disease state or therapeutic outcome over miRNAs or mRNAs, which participate only in the upstream pathways, due to the active participation of proteins in immune-tumor crosstalks^{66–69} and their functional role in a given pathway and can also reflect the state of their origin cell.^{70,71} These proteins are generally on the surface of the cells and quite often also on the EVs, which can be actively involved in intercellular communication.

Since EVs emulate numerous characteristics of their parent cells and carry specific antigens, they can precisely target specific cells and tissues, aiding in extended-distance communication and the transport of specialized materials. Several analytical tools have been developed to map the accessible surface proteins on the EVs from various sources,^{72–77} as well as their intercellular targets. Intriguingly, this capability offers a compelling inspiration for EV surface protein characterization technologies not just for diagnostics to look at overexpressed cancer markers but also for therapeutics to design and use them to target tissue.^{18,19,78–80} The designing is done depending on the hydrophilicity or hydrophobicity of a drug such that it can be encapsulated within EVs, or sequestered within the lipid bilayer of EVs, guided by surface markers to its target tissue, allowing for precise delivery and evasion of the host immune system.^{19,80–83} The same can be done with LPs as many cells express receptors for them, and hydrophobic cargo or drugs can be transferred inside them.^{84,85} Both EVs and LPs are biocompatible and stable and allow for targeted delivery, albeit with a greater focus on EVs due to their greater flexibility.

Moreover, EVs have been implicated in tumor proliferation and microenvironment modulation. For instance, individuals with prostate cancer have been observed to possess elevated concentrations of exosomes in their plasma and serum compared to healthy controls.⁸⁶ The presence of PD-L1 on exosomes derived from neoplastic cells has been identified, allowing such tumor cells to modulate cytotoxic T lymphocyte activity and potentially attenuate the efficacy of immunotherapeutic interventions.⁸⁷ In a therapeutic context, there is an observed upregulation of PD-L1 exosome production by malignant cells in response to anti-PD-L1 agents, hypothesized to contribute to a suboptimal patient therapeutic response.⁸⁸ Consequently, PD-L1-expressing exosomes may serve as a salient biomarker for monitoring responses to anti-PD-L1 therapy. Similarly, EVs overexpressing HER2 have implications in therapeutic resistance mechanisms, particularly against trastuzumab treatment in breast cancer,⁸⁹ highlighting the need for convenient, high throughput, and fast EV characterization methods for designing and monitoring therapy.

Additional major focuses in the quantification of EVs/LPs are not just the abundance of proteins associated with them but also in harnessing the information about their parent cells non-invasively. Beyond mere quantification, it is essential to grasp the dynamic intricacies of these associated proteins, including their

conformational states to their activity states. Discerning whether specific proteins, such as integrins,^{90–93} G Protein-Coupled Receptors (GPCRs),^{94,95} Matrix Metalloproteinases (MMPs),^{39–41,52–54,96,97} and Epidermal Growth Factor Receptor (EGFR)⁹⁸ on EVs, are in their active or inactive states can provide crucial insights into the cellular functions and mechanisms they are involved in such as the cellular pathways that trigger conformation/activity. Integrins, for instance, play a significant role in cell adhesion and signaling exist in several forms and conformations, are capable of sending bi-directional transmembrane signals,^{71,90,91,93,99–102} and have several forms present on EVs.^{38,54,71,95,103–106} Their presence and state on EVs can be indicative of cellular migration patterns or tissue repair processes, as well as pathways that trigger them. On the other hand, GPCRs, which are a large family of cell surface receptors, can signal cellular responses to external stimuli.⁹⁴ Tracking their active or inactive conformations on EVs could give insights into how a cell is responding to its environment, which can be especially crucial in understanding pathological conditions like cancer or inflammation.⁹⁴ Other examples include the Epidermal Growth Factor Receptor (EGFR) on EVs that are present in active/inactive states as well and are a biomarker in several cancers.^{72,86,98,107,108} Paraoxonase 1 on HDL is another example that is only active in their LP-bound conformation,¹⁰⁹ and we have shown that it is a significantly better marker than total PON1 in plasma in diagnosing coronary artery disease (CAD).¹¹⁰ Furthermore, post-translational modifications, such as phosphorylation or glycosylation, can further modify the function and localization of these proteins, providing additional layers of complexity to their role in EVs/LPs.¹¹¹ Other information about these proteins includes their isoforms, such as apolipoprotein E4 isoform on HDL, which is significantly upregulated in neurodegenerative patients.^{112,113} Similarly, we have also shown that conformationally active EGFR (aEGFR) (mab806) performs significantly better than ligand-mediated active EGFR (cetuximab) in diagnosing glioblastoma.⁹⁸ Therefore, we need to focus not just on the abundance but also on the state of the proteins on EVs.

While quantification is essential for EVs and LPs, the methodology and technology for their characterization are still behind and face significant challenges in order to study EVs and LPs robustly from real complex samples and be viable in clinical settings.^{98,110} Our focus in this review is to showcase how an ion-selective membrane sensing platform (ExoLP-Dx) overcomes several of the challenges associated with the quantification of EV/LP surface markers while also underlining the major challenges associated with their quantification.

A. Challenges in EV and LP quantification: Isolation, colocalization, bias, and non-specificity

The direct quantification of extracellular vesicles (EVs) and lipoproteins (LPs) in complex biological samples without prior isolation poses significant challenges. These samples replete with proteins, lipids, nucleic acids, and other entities can obscure and interfere with the accurate detection of EVs and LPs.^{114,115} Instruments and assays can be overwhelmed by the high concentration of non-target particles, while entities of similar size to EVs and LPs, such as chylomicrons or protein aggregates, can produce false signals in size-based detection methods such as Nanoparticle

26 May 2025 19:54:44

Tracking Analysis (NTA).^{114,115} Additionally, proteins of interest on the surface of EVs and LPs might have their signals masked by non-EV and non-LP fractions.⁵⁵ This interference further complicates the task, as it can lead to underestimation or even misidentification of the target.

Therefore, quantitative assessments of EVs and LPs frequently necessitate an initial isolation step, typically ultracentrifugation or immunoseparation techniques.^{6,50,81,114,116} However, isolation increases the purity and concentration of proteins on EVs/LPs and reduces interfering agents, enabling traditional assays such as western blot and ELISA to identify/quantify the total protein concentration on EVs/LPs. However, they still pose new sets of challenges like the larger EVs/LPs carry more cargo than smaller EVs/LPs in that isolated fraction, thus biasing these bulk assays as well as the need for advanced and bulky equipment, specialized training, limited throughput, and practical application barriers associated with ultracentrifugation or other isolation methods. Additionally, many isolation methods lead to artifacts that mimic EVs with similar features, damage EV/LP structural integrity, cause sample loss, and lead to the co-elution of EV and LP fractions with one another and soluble fractions.^{117,118} If the purpose is to quantify surface markers on EVs/LPs, the goal should be to do it without any isolation, have enough sensitivity to detect it from plasma and cancer cell media often employed to study cancer, and be bias-free with respect to the EV/LP size.

Even with an isolation step involved, there is a need to assay the surface proteins of EVs intact without lysing them. Looking at multiple proteins on the surface of EVs, i.e., colocalization on EVs, allows for a deeper analysis of its parent cells. For example, looking at tissue-specific markers with upregulated oncogenic proteins can aid in determining the specific cancer type—markers such as NCAM or ASGR1 can suggest neuronal¹¹⁹ or hepatic¹²⁰ origin, while the simultaneous presence/colocalization of these tissue-specific markers with overexpressed cancer biomarkers^{20,40,72,75,121–123} such as EGFR may help predict a range of cancer types. This can be further enhanced by targeting specific conformations/different states of the protein using specific antibodies such as the conformationally active version of EGFR⁹⁸ greatly increasing the diagnostic potential. Additionally, the identification of another target could indicate the tumor environment by looking at, for example, pro-angiogenesis proteins, such as the extracellular matrix glycoprotein developmental endothelial locus-1 (Del1), that have their role in promoting tissue-specific angiogenesis in cancer progression.¹²⁴ In neurodegenerative diseases, neuronal markers such as NCAM¹¹⁹ colocalized with amyloid beta and phosphorylated tau^{111,113,119} proteins can provide a way to look at neurodegenerative diseases accurately. By analyzing such colocalizations, we can uncover the specific combinations of proteins that work synergistically in EV-mediated intercellular interactions or even metastatic markers of cancer.^{39,70} This can aid in identifying potential biomarkers for various diseases, understanding EV biogenesis's molecular mechanisms, and optimizing therapeutic strategies that utilize EVs. Finally, colocalization assay enables a normalization strategy to enhance measurement reproducibility, despite variations in the EV production rate and sample size. For example, the fraction of CD63-positive EVs that have an EGFR should be the EV number and sample size independent. In summary, there is a need to use methods that can look at the

colocalization of proteins on EVs and LPs and not just a single protein.

Traditional downstream methods, such as western blot and enzymatic immunoassays, are not ideal for detecting colocalization as they employ a lysing step. While one might argue in favor of enzymatic immunoassays for this purpose by using a sandwich scheme, they often lack sensitivity and can be disrupted by redox interference,^{125–128} such as lipids/antioxidants enriched in intact EVs and LPs. Newer methods, including nanoflow cytometry^{129–131} and exoview,^{132,133} purport to detect colocalization, but they are hindered by the non-specific signals from unbound fluorophores. Additionally, nanoflow cytometry is less effective for smaller EVs and LPs, and both techniques necessitate stringent isolation steps beforehand. The organic fluorophores employed in these new methods are further compromised by interference from protein autofluorescence, photobleaching, degradation, and non-specific absorption.^{134–136} More expensive semiconductor reporters such as quantum dots are not as susceptible to interference from autofluorescence than organic fluorophores but still suffer from false positives due to non-specific adsorption.¹³⁷ Therefore, the challenge is not only to quantify EVs/LPs directly from complex biological samples but also to develop a suitable method that does not suffer from the typical drawbacks of traditionally used methods—such as redox interference from lipids, signal coming from non-specifically attached reporters, and last, an interference-free signal from untreated complex biological media, such as plasma and serum. This drove our lab to put significant efforts into developing ExoLP-Dx, and we will describe how ExoLP-Dx overcomes these challenges.

II. ION-EXCHANGE MEMBRANE EV/LP IMMUNO-SENSORS (ExoLP-Dx)

We have recently developed an ion-exchange membrane sensor to directly quantify highly charged molecules like nucleic acids and endotoxin,^{138–143} while weakly charged proteins,¹⁴⁴ EVs⁹⁸ and LPs,¹¹⁰ using a charged silica nanoparticle reporter approach in untreated biological samples. We review here why this electrokinetic membrane immunosensor (ExoLP-Dx) can overcome the various obstacles that listed in Sec. IA.

A. Working principle behind membrane sensors: Why go with charge?

Charge sensing provides notable advantages over traditional colorimetric or fluorescent methods. Many proteins that interfere with these traditional methods are weakly charged and do not produce a strong signal in charge sensing.¹⁴⁴ However, these proteins can interfere with colorimetric or fluorescent methods due to aromatic amino acids such as tryptophan, tyrosine, and phenylalanine.^{145–147} Furthermore, several amino acids on proteins have oxidative or anti-oxidative properties,¹⁴⁸ meaning that they can influence electron transfer in electrochemical sensing techniques. To navigate these challenges, membrane sensor was designed to use charge sensing but utilize ion transfer over electron transfer.^{98,110,138–141,143,144} This minimizes the complications of electrochemical sensing, which uses electron transfer or enzymatic immunoassays and reduces potential interference from

26 May 2025 19:54:44

redox reactions with the enzymatic proteins/lipids of the EVs/LPs or the redox agents present in biological media.^{125–127}

Charge sensing is typically connected with field-effect transistors (FETs),¹⁴⁹ which has not found significant application even though it has been around for 20 years. Fabrication cost is often a concern with microelectronic or nanoelectronic FET sensors. While highly sensitive, like electrochemical sensors, the electrical signal of the FET sensor is severely affected by the ionic strength and the Debye screening length, making it difficult to tune. The Debye length is less than a few nm in high-ionic strength physiological samples, thus rendering most of the charge of the EVs/LPs undetectable by the sensor. Recent efforts to resolve this Debye screening effect are largely unsuccessful or too elaborate to be practical.¹⁵⁰ More importantly, the detectable charge of each EV is a function of ionic strength of the buffer, which is difficult to control. In addition, the EV charge is a function of pH, making it difficult to calibrate for fluids like urine, whose pH can fluctuate between 5 and 8. We have, hence, designed a new charge-based sensor to overcome these limitations.

Our charge-based sensor is based on ion current through an anion-selective membrane [Figs. 1(a) and 1(d)]. It is the same low-cost ion-exchange membrane used in desalination and wastewater treatment.^{142,151,152} With a direct current (DC) bias, a counterion flux through the membrane disrupts the equilibrium Donnan potential jump across the membrane surface. Since the counterion flux exceeds the co-ion flux in an ion-selective membrane, there is a net flux of total ions across the membrane [Fig. 1(c)]. The result is an external concentration polarization phenomenon with ion depletion on one side of the membrane (entry side for the counterion) and ion enrichment on the other. The depletion zone can reach de-ionized (DI) water ionic strength and introduces the highest resistance to ion current flux through the membrane. The ion depletion action is very long-range—spanning a depletion region roughly the size of the membrane or even through an entire channel if the membrane is sufficiently large.^{142,151,152} The resistance of the membrane increases dramatically in this limiting current region introduced by ion depletion [Fig. 1(b)]. Since the charge analytes are associated with the probes, they are not mobile and cannot produce a resistive signal in the depletion zone. However, at a sufficiently high voltage, the depletion becomes so severe that the potential in the depletion region is below the Donnan potential of the membrane.¹⁵³ The resulting negative field pulls out some mobile charge from the membrane to maintain a monotonic gradient in the potential to sustain a current through the membrane. As this amount of external space charge is proportional to the normal field, it is a non-equilibrium-induced charge phenomenon that is different from the classical equilibrium space charge in the Debye layer that compensates for the surface charge. This external space charge buildup can partially screen the normal field to produce a tangential field and a tangential-induced electroosmotic flow. For membranes with a curved membrane, the induced space charge and electroosmotic flow vary along the surface such that some flow will be deflected in the normal direction to produce vortex pairs.¹⁵⁴ For flat membranes, a vortex pair train instability can appear spontaneously. This vortex instability convectively enhances the ion flux to reduce the resistance to produce an overlimiting

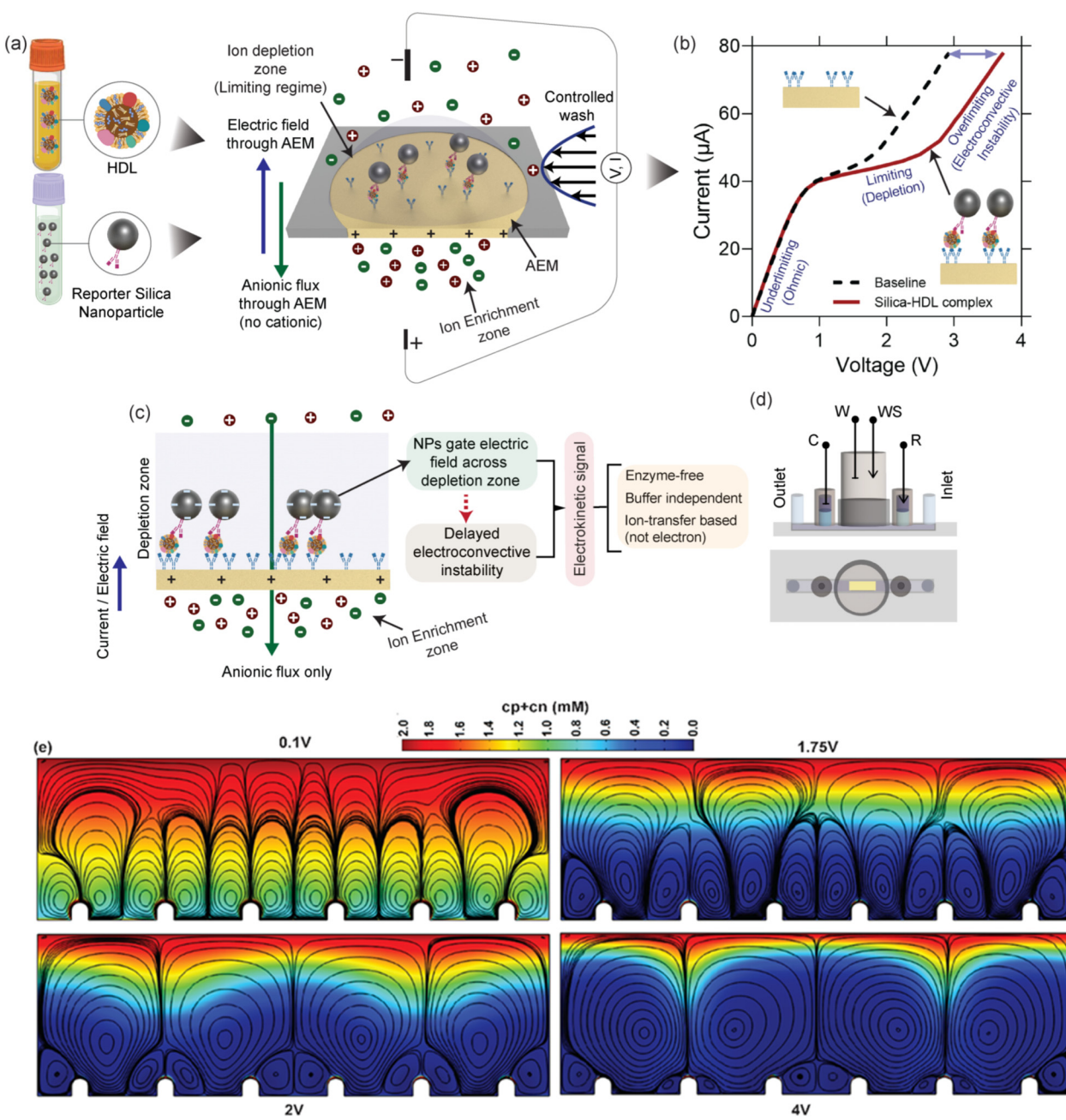
current. As this electroconvective instability involves a tangential electroosmotic flow, the presence of surface charges can sensitively control the onset voltage [Fig. 1(e)]. Since the overlimiting current transition occurs in the DI water condition of the depleted region, surface charges are minimally screened. Moreover, the sensitivity of the electro-convective instability to surface charges and the sensitivity of the ion current to convection in the depletion layer further amplify the detection signal and sensitivity. With additional design strategies, we can, hence, harness this uniquely non-equilibrium phenomenon for charge-based sensing to avoid major hurdles of EV quantification and significantly improve the signal-to-noise (S/N) ratio.

B. Maximizing the signal in S/N ratio: Silica nanoreporters and bias mitigation in EV/LP analysis

The signal-to-noise (S/N) ratio is critical in deciding whether a platform can characterize its target in complex biological samples and significantly affects its limit of detection and dynamic range. Maximizing the signal while minimizing noise is the go-to strategy for any biosensor,^{155–158} as one would aim to register a signal even when a smaller fraction of probes are occupied. The signal component is the signal produced by only the target, which we want to maximize, while the noise part is determined by interference from soluble proteins, non-specific binding of reporters, and non-targets to the surface. This section will discuss the signal component, while the noise component is discussed in Sec. II C.

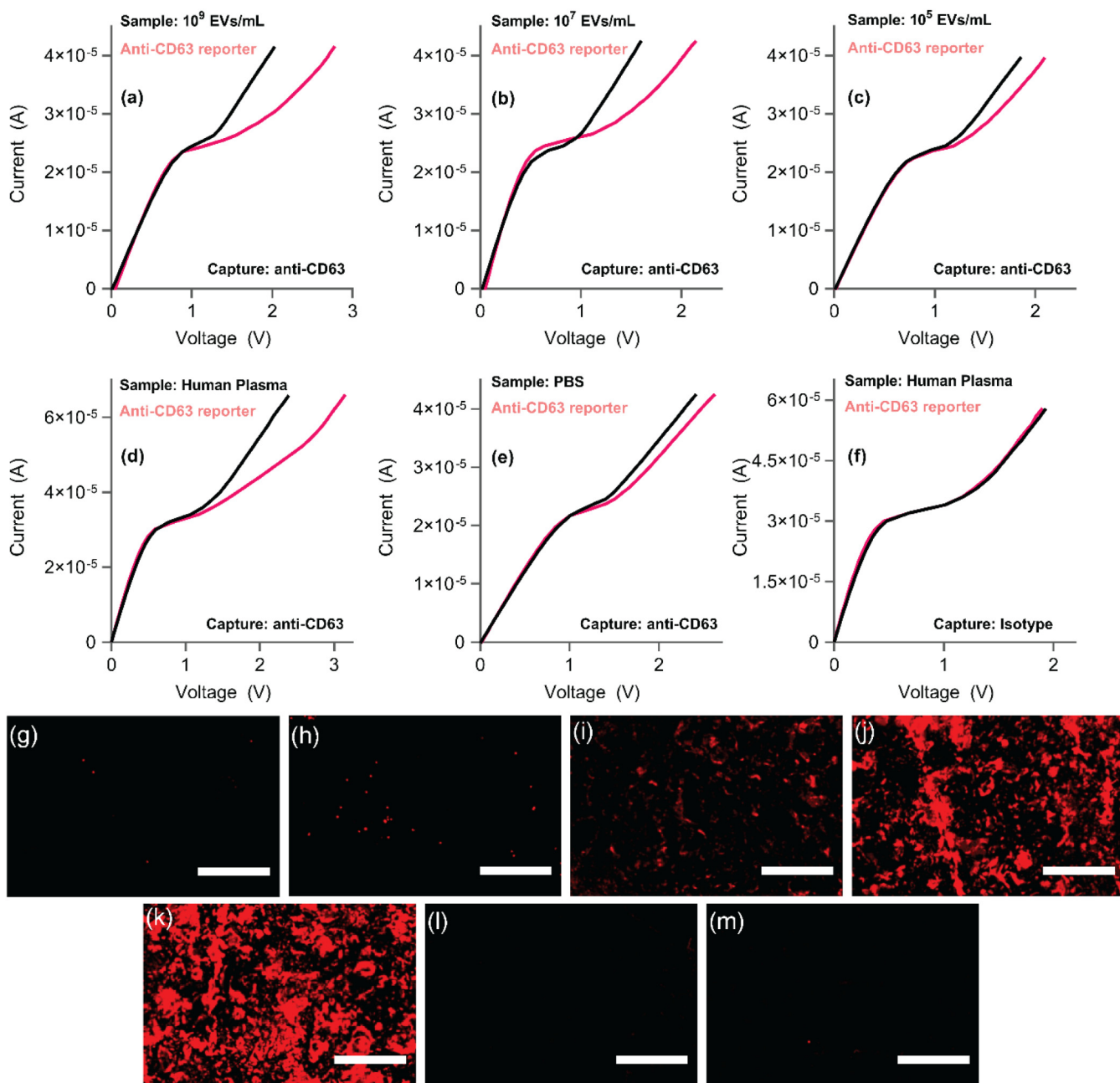
Like most proteins, EVs and LPs are weakly charged, with a zeta potential of about -20 mV ;^{98,159} they do not produce a signal by themselves on the membrane sensor as the sensor is only sensitive to charge. Therefore, even though the membrane sensor immunocaptures a protein on EVs or LPs, it does not produce any signal [Fig. 1(b)].^{98,110} Similarly, for complex biological samples, such as plasma and serum, although the sensor captures the proteins on non-EV/non-LP fractions or non-specifically adsorbs soluble proteins like albumin the sensor does not produce any significant signal. This unique charge sensitive characteristics of our membrane sensor, hence, allow us to directly use the plasma samples without requiring any prior sample pretreatment. After this, we incubate our membranes with silica nanoparticle reporters with a zeta potential of -50 to -40 mV toward a second protein on the EVs/LPs. This allows us to achieve two things—first, we are able to produce a signal only from EV/LP fractions without interference from its soluble counterparts, and second, the signal comes from the colocalization of two proteins on EVs/LPs, which is one of the major objectives in EV/LP characterization. Figures 2(a)–2(c) show varying concentrations of EVs with limit of detection lower than 10^5 EVs/ml .

Additionally, the size of the silica reporters is essential. Unlike conventional colorimetric or fluorescent signals, the size of silica particle can be adjusted over a broad range (10–1000 nm). Larger particles yield stronger signals due to the increased surface area, but a smaller dynamic range due to fewer reporters can be accommodated over the membrane surface. To achieve a maximum signal and ensure an optimal dynamic range for the sensor, we have selected a silica nanoparticle reporter size of 50 nm. This size is of the order of the Debye layer length prevalent under DI conditions,



29 May 2025 19:54:44

FIG. 1. (a) The positively charged anion exchange membrane (AEM) only allows anions to pass, with capture antibodies covalently linked to its surface for sensing. The controlled wash removes non-specifically bound species. (b) A general current-voltage characteristics curve showing the shift after the addition of sample and silica reporters that allows target quantification. (c) Mechanism for the electrokinetic signal produced in the ExoLP-Dx platform. The charged nanoparticles gate the electric field across the depletion layer leading to a delayed electroconvective instability. (d) Schematic of microfluidic chip used in our work. The inlet is connected to a pump to push samples and wash buffers. The middle reservoir houses a positively charged anion exchange membrane (AEM). Working W and counter C electrodes apply an electric field that passes from the middle reservoir into the microfluidic channel creating a depletion zone on the side facing the microfluidic channel. Working sense WS and reference R electrodes measure the voltage difference across the membrane. Reproduced with permission from Kumar *et al.*, *Nat. Commun.* **14**, 557 (2023).¹¹⁰ Copyright 2023 Author(s), licensed under a Creative Commons Attribution (CC BY) license. (e) Asymmetric bifurcation of microvortices and transition to OR with vortices in the ohmic region (0.1 V), near the transition to overlimiting region (1.75 V, 2 V) and overlimiting region (4 V). Reprinted with permission from Sensale *et al.*, *J. Phys. Chem. B* **125** (7), 1906–1915 (2021).¹³⁹ Copyright 2021 American Chemical Society.



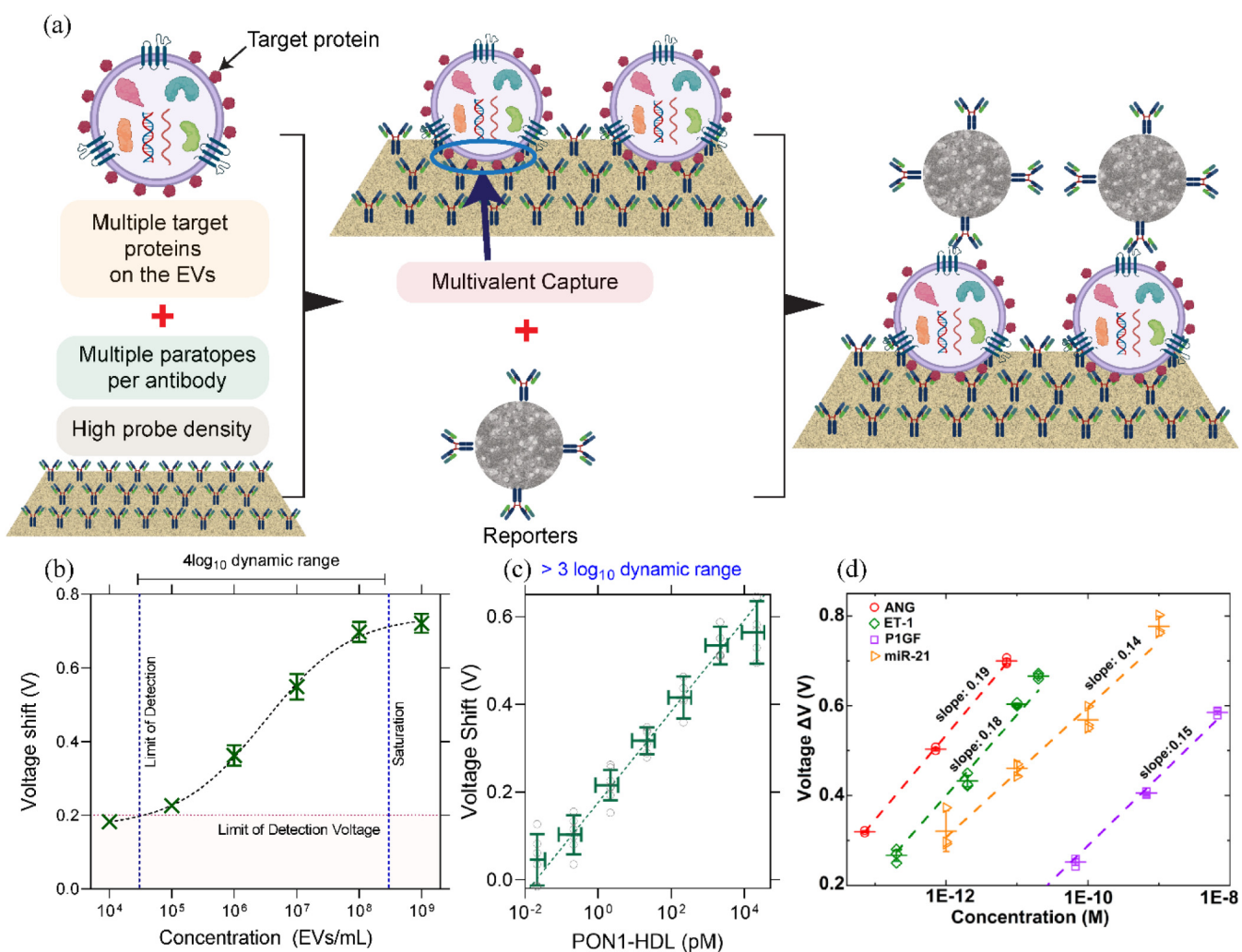
29 May 2025 19:54:44

FIG. 2. (a)–(c) The voltage shift associated with known amounts of EV using both anti-CD63 capture and reporter. (d) and (e) The results using human plasma and PBS as positive and negative controls, respectively, highlighting a minor shift caused by the EV-free PBS sample. (f) reveals that the shift induced by human plasma is minimal when using the isotype control capture antibody. EVs were sourced from a DiFi cell-conditioned medium. The lack of signal from isotype control using human plasma as a sample in (f) demonstrates the robustness of our sensor emphasizing the high signal-to-noise ratio. Reproduced with permission from Maniya *et al.*, Commun. Biol. **7**, 677 (2024).⁹⁸ Copyright 2024 Author(s), licensed under a Creative Commons Attribution (CC BY) license. (g)–(k) incubated with increasing concentrations of HDL (1 pM, 10 pM, 100 pM, 1 nM, 10 nM) and incubated with total HDL fluorescent silica reporter. (l) Silica particles on the overall surface at our membrane surface and the ability of ExoLP-Dx to have a very high signal-to-noise ratio. (l) and (m) Negative controls with (l) using solubilized proteins as control and (m) using wrong capture antibody (anti-ApoB).¹¹⁰ Reproduced with permission from Kumar *et al.*, Nat. Commun. **14**, 557 (2023).¹¹⁰ Copyright 2023 Author(s), licensed under a Creative Commons Attribution (CC BY) license.

which extends from 100 to 1000 nm. Notably, after binding to larger EVs/LPs, it continues to reside within the Debye layer, effectively gating the electric field due to its surface charge. With this, we can register a signal three standard deviations above the limit of blank when there is roughly one silica nanoparticle present every $20 \times 20 \mu\text{m}^2$ on the membrane surface or less than 1000 total silica nanoparticles on the membrane [Fig. 2(g)], thus allowing us to register a signal with less than 1000 EVs/LPs getting captured on the surface with a fM-pM bulk concentration with a large dynamic range [confocal images in Figs. 2(g)–2(k) correspond to the calibration plot in Fig. 3(c)]. In perspective, enzymatic immunoassays and western

blot require three to four orders of magnitude higher bulk concentration (pM to nM)^{160–162} since the reporter molecules do not produce a strong enough signal. Last, we do not prefer smaller reporters since we produce weaker signals per EV/LP. Additionally, it is easier to wash non-specifically bound silica using simple flow due to the large drag force experienced by them, as discussed later.

Moreover, since the silica nanoparticle reporters will repel a second reporter binding to the LPs/EVs over their Debye length (~ 100 –1000 nm under DI conditions), it also prevents a bias by reporting uniform signal from all targeted LPs/EVs irrespective of their size—these plaque western blot, enzymatic immunoassays and



26 May 2025 19:54:44

FIG. 3. Universality in ExoLP-Dx. (a) Multivalency on EVs can lead to mass-transfer limitation due to multivalent capture, multiple binding sites, and low diffusivity of EVs ($\text{Da} \gg 1$). Schematic shown for EVs but true for LPs as well. (b) CD63 capture and CD63 reporter. Reproduced with permission from Maniya et al., Commun. Biol. 7, 677 (2024).⁹⁸ Copyright 2024 Author(s), licensed under a Creative Commons Attribution (CC BY) license. (c) ApoAI-capture and ApoAI reporter with the fM-pM limit of detection using ExoLP-Dx. Reproduced with permission from Kumar et al., Nat. Commun. 14, 557 (2023).¹¹⁰ Copyright 2023 Author(s), licensed under a Creative Commons Attribution (CC BY) license. (d) Universal slope observed for multiple tissue proteins and also consistent with (b) and (c). Reprinted with permission from Sensale et al., J. Phys. Chem. B 125 (7), 1906–1915 (2021).¹³⁹ Copyright 2021 American Chemical Society.

even proteomic approaches since larger EVs/LPs will carry more cargo, thus masking the effects of other smaller EV/LP populations.

C. Minimizing the noise in S/N ratio: Controlled wash to enhance specificity

Our platform's design emphasizes optimizing the signal-to-noise (S/N) ratio. This involves a delicate balance between enhancing the signal and minimizing unwanted noise, a crucial aspect of our main objective of directly quantifying extracellular vesicles (EVs) from complex media such as plasma without sample isolation. One primary challenge in biosensor operation arises from non-specific protein binding on surfaces driven by hydrophobic interactions. This sometimes includes non-EV/non-lipoprotein (LP) fractions that possess the target protein, resulting in misleading signals. It is worth noting that while non-specific protein binding does not produce a signal with our membrane sensor, it can pave the way for silica nanoreporters to bind, especially if the target protein is abundant in non-EV/non-LP fractions that non-specifically bind to the surface. In traditional assays, detergents are used to counteract non-specific binding, but their use with EVs is limited as they can disrupt lipid bilayers, leading to EV lysing—something we want to avoid, as discussed before. Fortunately, our membrane, due to being of hydrophilic nature, reduces the need for such detergents, significantly reducing such non-specific interactions with the surface.

The second issue concerns the physical behavior of antibodies on the surface. Due to van der Waals forces, antibodies often exhibit an affinity for a broad spectrum of substances. However, their strongest attraction is unequivocally reserved for their primary target. This widespread affinity means that many proteins have the potential to bind non-specifically to antibodies, a process driven by both van der Waals and sometimes even potential electrostatic interactions between the two. It is worth noting that non-specific antigens, when bound to an antibody, generally display an off-rate¹⁶³ of 0.01 s^{-1} compared to their targets, typically 0.0001 s^{-1} . This suggests that a wash of around 1 min effectively mitigates these unsought interactions without removing the targets. In fact, with a higher ionic concentration buffer, this off-rate driven wash is reduced to only about 10 s since the off-rate at higher ionic concentration is increased due to the Debye screening of electrostatic attractions. Therefore, with the use of a high-conducting wash buffer, like phosphate-buffered saline (PBS) for a minute, the vast majority of non-specific targets to the antibodies can be removed. We can utilize a similar strategy to differentiate HER2 from its isomer,¹⁶⁴ with a similar equilibrium immuno-dissociation constant as well as different serotypes of dengue virus,¹⁴³ by using a similar wash methodology due to the difference in the off-rate of the isomers/serotypes.

The last and perhaps the most important optimization resides with the silica nanoparticle. The first two issues are problematic because they can potentially create binding sites for silica nanoparticles by letting the targeted protein on non-EV/non-LP fraction non-specifically bind to the surface/antibody; however, the signal is always produced by the silica nanoparticle reporter. Silica nanoparticle reporter can also non-specifically bind to the surface. Nonetheless, our size selection for nanoparticle reporters ensures that removing non-specifically bound silica on the surface is

possible using simple shear flow with higher ionic concentration buffers to weaken the electrostatic interactions. This stands in contrast to platforms using fluorophores or enzymes; their small size makes them very resistant to removal by drag force.

Therefore, the microfluidic chip platform allows us to include a flow component in the assay protocol rather than buffer replacement in batches since the latter do not have significant drag applied to the surface. We employed a wash step of about a minute to allow for off-rate mediated removal of non-targets and employed high-ionic concentration buffers to screen electrostatic interactions—all without relying on detergents and without any surface passivation of the membrane sensor. Adopting this approach, we have successfully approached the limit of detection to the thermal noise of approximately 50 mV, as observed in blank experiments and isotype controls, allowing us to observe a discernable signal with $\sim\text{fM}$ levels of EVs/LPs [Figs. 3(b) and 3(c)]. This also allows us to have a larger dynamic range and look for subfractions in as small as 0.01% of the EVs. In general, we use $4\times$ PBS for 10 s and $1\times$ PBS for 60 s to screen any electrostatic attraction between the oppositely charged nanoparticle and membrane surface and to increase the off-rate of the non-target dissociation. We, hence, have achieved a robust, interference-free, and sensitive EV sensor. The remaining issues are normalization due to endogenous variability in the EV concentration and variations due to long transport-controlled irreversible association. Figure 2(d) shows that while human plasma with CD63 capture and reporter produces very high signals, its isotype control [Fig. 2(f)], blank [Fig. 2(e)], soluble proteins [Fig. 2(l)], or non-target antibody [Fig. 2(m)] does not produce any significant signal showing minimal noise in ExoLP-Dx.

D. Probe affinity independence: Using transport limitation over kinetics and fast pseudo-equilibrium

Antibody–antigen binding is commonly modeled as an equilibrium reaction, using the forward on-rate k_{on} and backward off-rate k_{off} . The dissociation constant, K_D , is defined as $k_{\text{off}}/k_{\text{on}}$. While this model is universally recognized, it often overlooks the transport dynamics, such as how antigens must diffuse to the antibody-functionalized surface. A more comprehensive model integrates these transport limitations^{108,161} with the antibody–antigen kinetics, introducing the concept of a rate-determining step. The slower two processes dictate the reaction rate: transport or binding kinetics. This relationship is expressed by the Damköhler number, which is the rate of reactive to diffusive flux, $Da = k_{\text{on}}C_{\text{probe}}\delta/D$, where δ represents the characteristic depletion layer length scale and D denotes the diffusivity of a target, like EVs or LPs.

If $Da \gg 1$, transport is the rate-limiting step. On the other hand, if $Da \ll 1$, the binding kinetics becomes the bottleneck. Operating in a regime where $Da \gg 1$ has advantages: it reduces the reliance on kinetic parameters linked to antibodies, addressing the reproducibility challenges that have long vexed researchers. However, this also introduces a bias as the diffusivity of EVs/LPs can vary over an order and lead to larger EVs/LPs having a smaller flux than the smaller EVs/LPs, leading to surface capture not being representative of the bulk. We overcome this by maintaining a Peclet number $Pe = 0$ during incubation. In this 3D point sensor

26 May 2025 19:54:44

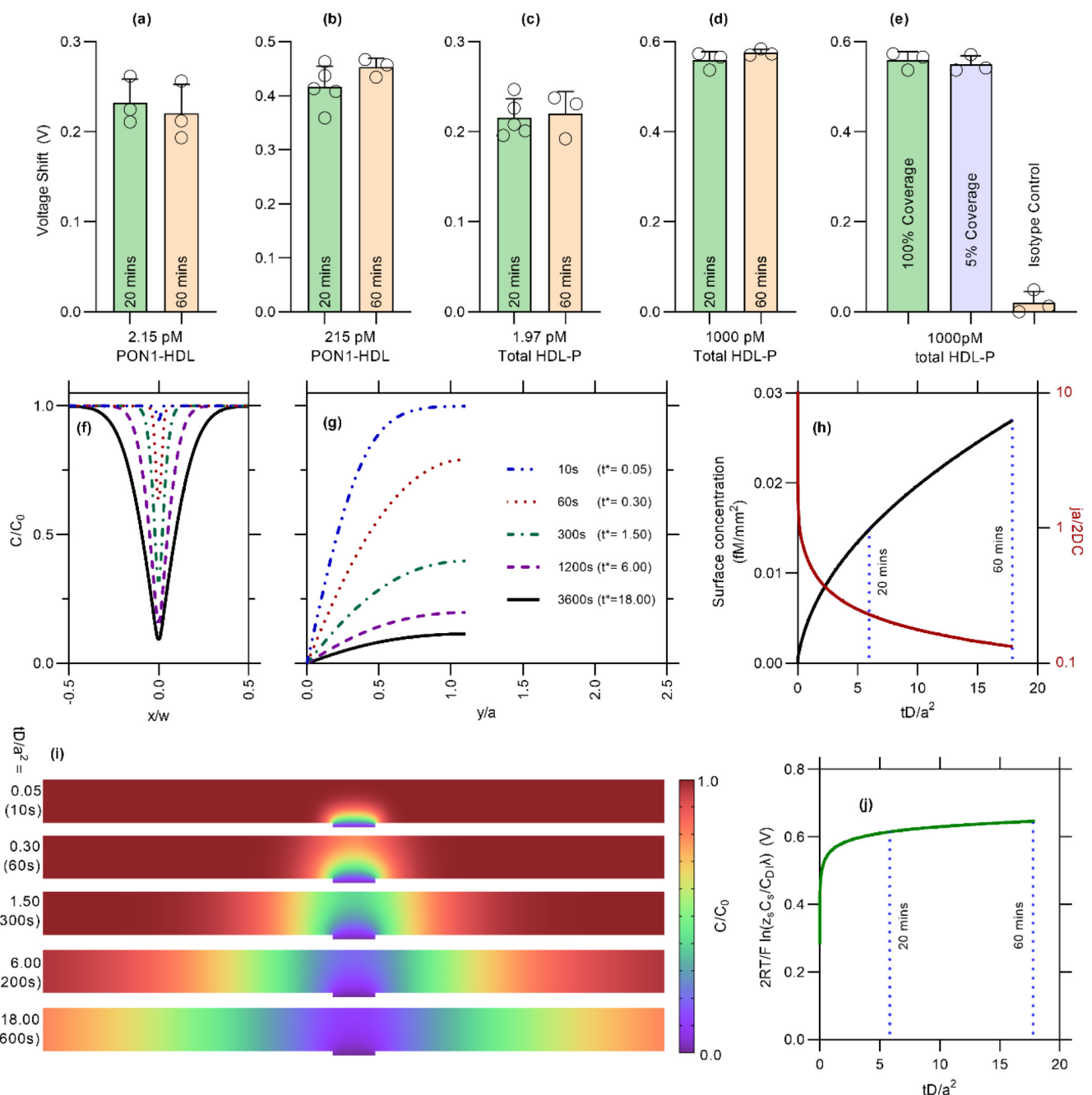


FIG. 4. Mass-transfer limitation in ExoLP-Dx: (a)–(d) Signals at various times for 2.15 pM PON1-HDL, 215 pM PON1-HDL, 1.97 pM HDL-P, and 1000 pM HDL-P, with identical signals between 20 and 60 min. (e) The influence of antibody surface coverage on the overall signal with 100%, 5%, and 0% coverage; the similarity between 100% and 5% indicates a mass-transfer limited regime from the probe density independence. (f) and (g) Concentration at the channel's center, both along the channel and directly above the membrane (with the membrane at origin), and the decreasing concentration gradient over time; a shared legend for both is in (g). (h) The analyte's surface concentration on the membrane and the non-dimensional flux over time. (i) Zoomed-in images of the microfluidic channel from numerical simulations, showcasing an irreversible reaction on the membrane in a mass-transfer limited regime. (j) The theoretical signal progression over time, indicating a pseudo-steady state after $t^* = 1$. For reference, each scenario in (a)–(e) was measured independently three times, except for 20 min cases in (b) and (c), which were measured five times. Error bars denote one standard deviation. The same sample was consistently assessed at each specific concentration on different ExoLP-Dx sensors. Reproduced with permission from Kumar *et al.*, Nat. Commun. **14**, 557 (2023).¹¹⁰ Copyright 2023 Author(s), licensed under a Creative Commons Attribution (CC BY) license.

limit with $Pe = 0$ and $Da \gg 1$, the radially focusing diffusive flux toward the sensor rapidly produces a depletion zone of all the targets within a few sensor radii from the sensor. So even though the larger particles will diffuse to the surface slowly, all the targets in a given volume (few sensor radii from the sensor) will be depleted irrespective of their diffusivity, thus keeping the surface captured proportions of different-sized EVs as representative of the bulk. Additionally, since the depletion volume is controlled by the sensor size, it does not require us to have very precisely fabricated microfluidic chips, as the change in their dimensions does not change the signal. Moreover, the sample volume, irrespective of the input volume, is also guided by the sensor size, thus not requiring any complex pipetting or precise syringe or peristaltic pumps. We can only do this because the membrane sensor has enough sensitivity to perform these experiments in the static state and does not necessitate flow, exposing the sensing surface to a larger sample volume.

This also has an added advantage—a faster steady state. Since EV/LP depletion volume does not extend beyond the dimension of the sensor radius, a steady state is reached, where the flux to the sensor slows down considerably. Hence, a given fraction of EV within the depletion volume associates rapidly during this transient and additional EV flux to the sensor becomes negligible. This physical phenomenon is due to the converging diffusive flux lines of the point sensor. A steady state solution does not exist for weakly converging or non-converging cylindrical and planar geometries in an unbounded domain—a steady state is only achieved if all the analytes of the sample are depleted by the irreversible association reaction. We estimate the diffusion time to be ~ 20 min for our 500 μm membrane sensors

for EVs [see Figs. 4(f)–4(j)], and the voltage signal should not change appreciably after that. We have, indeed, verified experimentally that the signal does not change by more than one standard deviation several hours after this characteristic diffusion time [see Figs. 4(a)–4(d)]. Hence, the signal is from a fixed fraction of EVs within the depletion volume, which is only a function of membrane size and not the sample volume size. If we can fabricate the point sensors reproducibly with identical dimensions, the captured EVs are always from the same volume of fluids above the sensor.

Many properties of EVs/LPs and membrane sensors can help us achieve $Da = k_{on}C_{probe}\delta/D \gg 1$ at $Pe = 0$. For example, the diffusivity of EVs/LPs is several orders lower than the typical diffusivity of proteins, thus increasing Da while having a high probe density on the membrane surface also helps increase Da . Last, although one cannot always find high-affinity antibodies, the multiple copies of proteins on EVs/LPs can lead to multivalent capture of these proteins [as shown schematically in Fig. 3(a)]. For example, HDL has multiple ApoAI,¹⁶⁵ while EVs have multiple copies of tetraspanins¹⁶⁶ and some other markers, such as glycan 1 in cancer patients.¹⁶⁷ This, when coupled with high probe density, can lead to multivalent capture, i.e., multiple paratopes of antibodies on the membrane surface bind to multiple copies of the proteins on the EV/LP surface, leading to an avidity-enhanced k_{on} and k_{off} . All these factors can contribute to $Da \gg 1$, thus removing the biases as well as affinity dependence. $Da \gg 1$ can be verified experimentally in a variety of ways, but the easiest of which is to look at probe surface concentration dependence. If changing the probe concentration while keeping every other parameter fixed changes the overall signal, it implies that it is not in the transport limitation. However, if it is

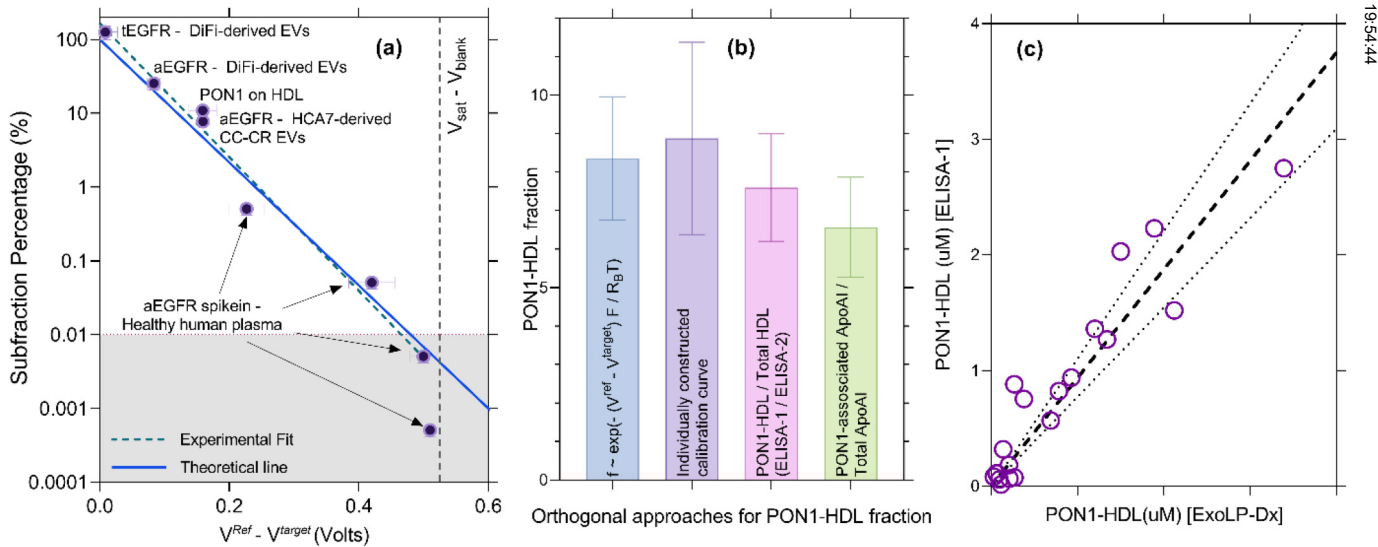


FIG. 5. (a) Universal scaling of ExoLP-Dx. (b) Comparison of orthogonal enzymatic immunoassays with universal scaling and individual calibration plots for PON1 on HDL. Reproduced with permission from Maniya *et al.*, Commun. Biol. 7, 677 (2024).⁹⁸ Copyright 2024 Author(s), licensed under a Creative Commons Attribution (CC BY) license. (c) For 20 human plasma samples, a comparison of PON1-HDL concentration from an orthogonal method (ELISA-1) from ExoLP-Dx. The orthogonal method took >24 h, while ExoLP-Dx took 30 min for the same characterization. Reproduced with permission from Kumar *et al.*, Nat. Commun. 14, 557 (2023).¹¹⁰ Copyright 2023 Author(s), licensed under a Creative Commons Attribution (CC BY) license.

26 May 2025 19:54:44

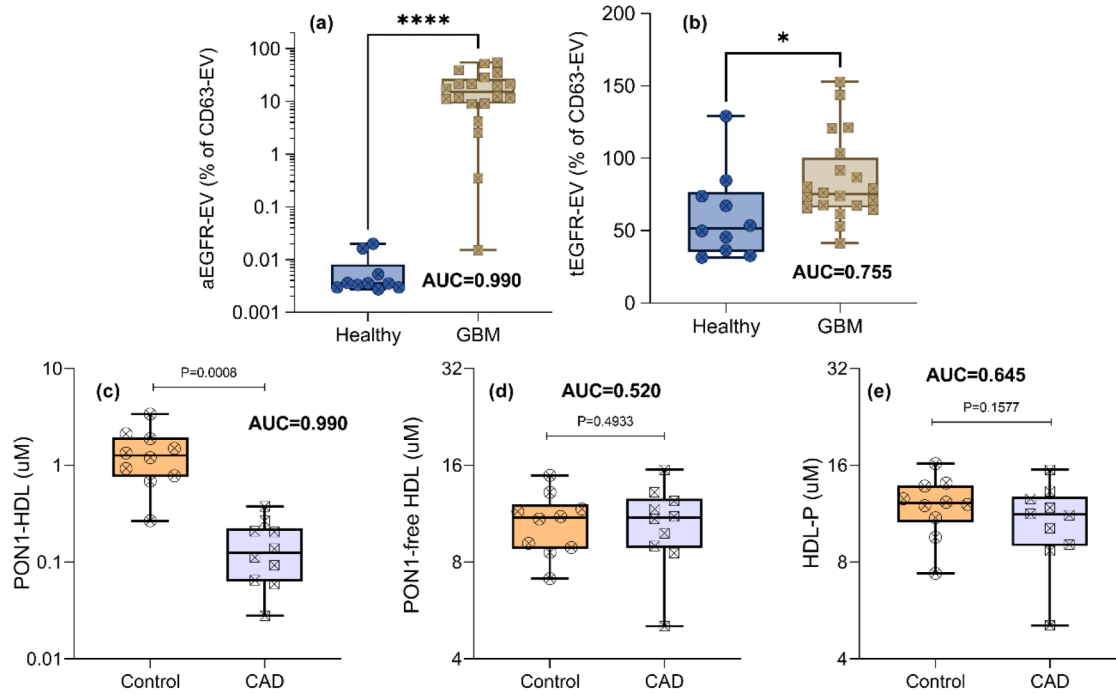
the other way around, it is in the transport limitation [Fig. 4(e)]. One must be careful when using 1-ethyl-3-(3-dimethylaminopropyl)carbodiimide hydrochloride (EDC)/N-hydroxysuccinimide (NHS) to alter the probe concentration as often the antibody is taken in large amounts, instead one can alter the probe density by using competing target antibodies with isotype control (while keeping total IgG constant) during EDC/NHS.¹¹⁰

E. Subfraction quantification: Universal scaling despite heterogeneity in complex media

The charged silica reporter produces a voltage shift in response to the Gouy-Chapman zeta potential, especially at high surface charge densities.¹⁶⁸ This voltage shift is influenced by the logarithm of the reporter's charge concentration. This logarithmic dependency of the voltage on either EV or reporter concentration accounts for its large dynamic range. If it had scaled linearly, a 4-log dynamic range would produce unrealistic thousand volt signals and would not be achievable due to the onset of other physical phenomena such as water splitting.¹⁴³ The essence of this logarithmic signal comes from Debye screening. Even after reducing the ion concentration close to that of DI water, some ions persist, screening the charged reporters.¹³⁹ The counterion concentration equals the reporter charge on the membrane surface. However, because of diffusion, more counterions accumulate toward the surface. On a highly charged surface,

this results in enhanced screening, consistent with the classical Boltzmann equilibrium theory for Debye screening, and it yields the scaling that the voltage signal scales as the logarithm of the reporter concentration.^{139,169} We have, indeed, found this logarithm scaling for signals produced by molecules captured by oligo or antibody probes on the membrane experimentally [see Figs. 3(b)–3(d)] as well for LPs¹¹⁰ and EVs.⁹⁸ Their standard curves all have the same slope in a semi-log plot. The observed shift is due to different affinity of the capture antibody-target or reporter-target association reactions. This large dynamic range facilitates the detection of incredibly small fractions, down to 0.01%. In practical terms, even if just 1 out of 10 000 captured EVs carries our target protein, it can still produce a signal discernible above the detection threshold as seen in the spike-in data of Fig. 5(a).

We selected the nanoparticle size so that only one reporter can occupy each EV/LP, independent of the EV/LP size, and also that the reporter of one EV does not interfere with the reporter association with another EV. As such, each reporter registers one EV with colocalized capture protein and reporter proteins. Additionally, because the concentration of reporters is typically $\gg K_D$, the reporting antibody also has probe affinity independence and saturates the EVs with target proteins that were captured producing a reporter probe affinity independent parameter. We can use this and logarithmic scaling to our advantage by proposing a universal scaling. Assuming that we are interested in the colocalization of proteins X



26 May 2025 19:54:44

FIG. 6. (a) and (b) Diagnosing Glioblastoma multiforme with conformationally active EGFR (mab806) over total EGFR (CTX) gives much better sensitivity using ExoLP-Dx. Reproduced with permission from Maniya *et al.*, Commun. Biol. 7, 677 (2024).⁹⁸ Copyright 2024 Author(s), licensed under a Creative Commons Attribution (CC BY) license. (c)–(e) Diagnosing coronary artery disease (CAD) with active PON1 on HDL over PON1-free HDL or total HDL, respectively, gives significantly better sensitivity, specificity, and area under the curve (AUC) values. Reproduced with permission from Kumar *et al.*, Nat. Commun. 14, 557 (2023).¹¹⁰ Copyright 2023 Author(s), licensed under a Creative Commons Attribution (CC BY) license. All were calculated using ExoLP-Dx.

and Y , we put antibodies for X on the surface and report with Y . Interestingly, if we were to normalize with a generic protein Z , which is most abundant on the target, it could act as a reference. If we write the equations, then $V^{\text{target}}|_X^Y = 2R_B T \ln(C_{X,Y})/F$ and $V^{\text{ref}}|_X^Z = 2R_B T \ln(C_{X,Z})$, where R_B , T , α are constants—universal gas constant, temperature, and constant related to zero potential reference and charge valency, respectively, and C_X^Y , C_X^Z are the surface captured concentrations of EV populations that contain proteins X and Y and proteins X and Z , respectively. This yields $C_X^Y/C_X^Z = \exp(-(V^{\text{ref}} - V^{\text{target}})F/2R_B T)$. Using Z as a standard marker like CD63 or ApoAI, this essentially measures the percentage of EVs or LPs with protein X that also contain protein Y . Since we are not dependent on any affinity, this ratio is also representative of the bulk. The semi-log plot of this normalized EV fraction with the disease marker is a universal standard curve independent of the total number of EVs.

By using an EV marker for capture and a disease marker for reporting, we can, hence, estimate the fraction of a particular family of EV that has the diseased markers. That both the capture and reporter association reactions are irreversible stipulates that the standard calibration curve of this fraction with respect to the voltage signal $\Delta V = V^{\text{ref}} - V^{\text{target}}$ is a universal one, where V^{ref} uses the capture antibody as the reporter antibody and V^{target} uses the

disease biomarker antibody. We are able to collapse the data for EVs and HDL on this universal calibration curve in Fig. 5(a). The spike-in data are obtained by the serial dilution of isolated EVs spiked into plasma. Only two voltage measurements are required to obtain the fraction of EVs, captured with an EV-specific marker, with a particular disease protein. We have compared our colocalized percentage obtained from the membrane sensor using universal scaling for PON1-HDL from several orthogonal methods providing similar values despite a significantly longer time (>24 h) compared to the membrane sensor (30 min) as seen in Fig. 5(b) as well as for 20 independent human samples directly from plasma compared to the orthogonal method [Fig. 5(c)]. This universality of all EVs/LPs data is strong evidence that the membrane sensor has overcome the myriad of heterogeneities in EV diagnostics with untreated plasma. Using our method, we successfully quantified various forms of EGFR, including the conformationally active EGFR (aEGFR) and the total EGFR (tEGFR) found on EVs [see Figs. 6(a) and 6(b)]. We also identified different versions of PON1, such as the active PON1 on HDL, PON1-free HDL, and total HDL [see Figs. 6(c)–6(e)]. Our findings show that focusing on the specific states and conformations of proteins, instead of just their abundance, can lead to significantly improved diagnostics when measured directly from plasma without bias.

26 May 2025 19:54:44

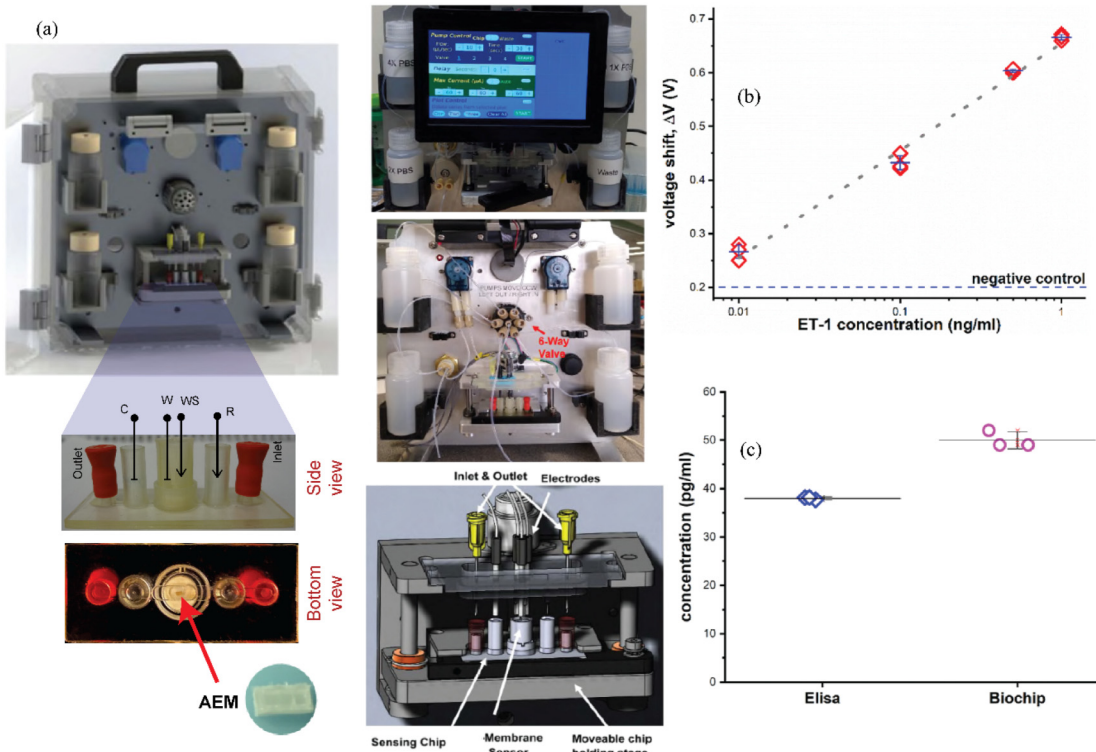


FIG. 7. (a) Automated prototype that can also run in multiplex mode with three sensors at a time. (b) and (c) Monitoring tissue marker ET-1 using a membrane sensor with benchmarking against ELISA. Reprinted with permission from Ramshani *et al.*, *Talanta* **225**, 122021 (2021).¹⁴⁴ Copyright 2021 Elsevier.

III. CONCLUSIONS AND FUTURE OUTLOOK

The primary objective of this review is to pivot the ExoLP-Dx domain from individual EV/LP analysis to bulk EV/LP assays that can overcome the various heterogeneity issues related to EV variation and complex samples. Our analysis primarily focuses on how membrane sensors provide a reliable means to quantify specific EV subclasses based on surface proteins. While it is feasible to conduct intra-EV protein assays, they must be fluorescence-based and necessitate a method for reporter insertion. Another approach involves lysing the EVs, although this may result in some analyte loss and may require some initial immunocapture to look at colocalization. An intriguing direction is to utilize surface-enhanced Raman spectroscopy (SERS) to obtain single-EV Raman spectrum of both surface and intra-EV proteins. While this technique is label-free and probe-free in theory, the abundance of EVs suggests that the immunocapture of a subset of EVs is necessary to enable the Raman characterization of a reasonable number of EVs. Consequently, an integration of the membrane sensor with an SERS setup and/or an optical reporter insertion protocol may offer the most comprehensive assay of the heterogeneous EV/LP families.

The EV membrane sensor, despite its potential, faces some commercialization barriers. The main challenge is the fabrication of the membrane sensor. While we have developed a 3D printing process for sensor fabrication, its mass production might best be achieved through injection molding. Incorporating *in situ* membrane synthesis can eliminate manual membrane assembly. We have also worked in that direction and recently developed an *in situ* membrane synthesis process.¹⁵⁴ Another noted shortcoming is the short shelf life of membrane-functionalized antibodies, typically around the half-life of the antibodies that are prone to proteolytic degradation. Ideally, biotinylated antibodies paired with pre-functionalized streptavidin membranes (which have longer shelf lives) should be used. Furthermore, we still need to fine-tune wash protocols for various EVs. The introduction of a surface acoustic wave module¹⁴¹ might minimize or eliminate the wash step, negating the need for a microfluidic chip, thus simplifying manufacturing.

In our continued research efforts, we have made progress in addressing the identified challenges. We have developed multiplex-enabled automated prototypes, as depicted in Fig. 7(a), and proceeded with validation using tissue markers, as shown in Figs. 7(b) and 7(c). These advancements aim to streamline the operation of membrane biochips. Our objective is to introduce a refined automated ExoLP-Dx capable of processing physiological samples, such as plasma, without the need for prior treatment. We anticipate that this could represent a notable shift in non-invasive screening methodologies, leveraging the capabilities of EV/LP-transported protein biomarkers.

ACKNOWLEDGMENTS

This work was partially supported by the NIH Commons Fund, through the Office of Strategic Coordination/Office of the NIH Director, under Grant No. 1UH3CA241684-01 (H.-C.C. and S.S.), the National Heart, Lung, and Blood Institute (NHLBI) under Award No. R01HL141909 (H.-C.C. and S.S.), and the NIH under Grant No. R21-HG009010-01 (H.-C.C and S.S.). S.K. would like to

thank the Berthiaume Institute for Precision Health (BIPH) for the 2023 O'Brien Endowment for Excellence Graduate Fellowship.

AUTHOR DECLARATIONS

Conflict of Interest

The authors have no conflicts to disclose.

Author Contributions

Sonu Kumar: Conceptualization (equal); Data curation (lead); Formal analysis (equal); Investigation (lead); Methodology (equal); Validation (equal); Writing – review & editing (equal). **Satyajyoti Senapati:** Conceptualization (equal); Formal analysis (equal); Funding acquisition (equal); Methodology (equal); Project administration (equal); Supervision (equal); Validation (equal); Writing – review & editing (equal). **Hsueh-Chia Chang:** Conceptualization (equal); Formal analysis (equal); Funding acquisition (equal); Methodology (equal); Project administration (lead); Supervision (equal); Validation (equal); Writing – review & editing (equal).

DATA AVAILABILITY

Data sharing is not applicable to this article as no new data were created or analyzed in this study.

REFERENCES

- ¹B. Sabatke, I. V. Rossi, A. Sana, L. B. Bonato, and M. I. Ramirez, "Extracellular vesicles biogenesis and uptake concepts: A comprehensive guide to studying host-pathogen communication," *Mol. Microbiol.* (published online) (2023).
- ²A. Kottorou, F. I. Dimitrakopoulos, G. Diamantopoulou, F. Kalofonou, M. Stavropoulos, K. Thomopoulos, T. Makatsoris, A. Koutras, and H. Kalofonos, *Cancers* **15**(6), 1685 (2023).
- ³A. Cruz Camacho, D. Alfandari, E. Kozela, and N. Regev-Rudzki, *PLoS Pathog.* **19**(2), e1011140 (2023).
- ⁴P. Fonseka and S. Mathivanan, *Cells* **12**(2), 280 (2023).
- ⁵Y. Jin, L. Ma, W. Zhang, W. Yang, Q. Feng, and H. Wang, *Biol. Res.* **55**(1), 35 (2022).
- ⁶N. Hadizadeh, D. Bagheri, M. Shamsara, M. R. Hamblin, A. Farmany, M. Xu, Z. Liang, F. Razi, and E. Hashemi, *Front Bioeng. Biotechnol.* **10**, 1019821 (2022).
- ⁷Y. Fang, Z. Wang, X. Liu, and B. M. Tyler, *Front. Microbiol.* **13**, 817844 (2022).
- ⁸S. Xie, Q. Zhang, and L. Jiang, *Membranes* **12**(5), 498 (2022).
- ⁹H. Wei, Q. Chen, L. Lin, C. Sha, T. Li, Y. Liu, X. Yin, Y. Xu, L. Chen, W. Gao, Y. Li, and X. Zhu, *Int. J. Biol. Sci.* **17**(1), 163–177 (2021).
- ¹⁰X. Zheng, M. Bähr, and T. R. Doeppner, *Int. J. Mol. Sci.* **20**(23), 5995 (2019).
- ¹¹L. Patras and M. Banciu, *Curr. Pharm. Des.* **25**(17), 1980–2006 (2019).
- ¹²S. Maacha, A. A. Bhat, L. Jimenez, A. Raza, M. Haris, S. Uddin, and J. C. Grivel, *Mol. Cancer* **18**(1), 55 (2019).
- ¹³N. O. Yamada, *Ann. Transl. Med.* **5**(3), 59 (2017).
- ¹⁴R. P. Madeira, L. M. Dal'Mas Romera, P. de Cássia Buck, C. Mady, B. M. Ianni, and A. C. Torrecilhas, *J. Immunol. Res.* **2021**, 6650670 (2021).
- ¹⁵M. Cafora, M. Hoxha, L. Cantone, V. Bollati, A. Pistocchi, and L. Ferrari, *Methods Enzymol.* **645**, 277–295 (2020).
- ¹⁶F. Royo, M. Azkargorta, J. L. Lavin, M. Clos-Garcia, A. R. Cortazar, M. Gonzalez-Lopez, L. Barcena, H. A. Del Portillo, M. Yáñez-Mó, A. Marcilla, F. E. Borras, H. Peinado, I. Guerrero, M. Váles-Gómez, U. Cereijo, T. Sardon, A. M. Aransay, F. Elortza, and J. M. Falcon-Perez, *Front. Cell Dev. Biol.* **8**, 613583 (2021).
- ¹⁷V. O. Silva, M. M. Maia, A. C. Torrecilhas, N. N. Taniwaki, G. M. Namiyama, K. C. Oliveira, K. S. Ribeiro, M. D. S. Toledo, P. Xander, and V. L. Pereira-Chioccola, *Parasite Immunol.* **40**(9), e12571 (2018).

26 May 2025 19:54:44

- ¹⁸P. Izquierdo-Alarcos, V. Moreno-Manzano, and V. Felipo, *Neural. Regener. Res.* **19**(1), 55–61 (2024).
- ¹⁹G. L. Liguori and V. Kralj-Iglc, *Cancers* **15**(18), 4425 (2023).
- ²⁰R. Gao and X. Li, *Adv. Exp. Med. Biol.* **1418**, 17–31 (2023).
- ²¹L. Y. M. Michel, *Int. J. Mol. Sci.* **24**(9), 7745 (2023).
- ²²E. Schoger, F. Bleckwedel, G. Germena, C. Rocha, P. Tucholla, I. Sobitov, W. Mobius, M. Sitte, C. Lenz, M. Samak, R. Hinkel, Z. V. Varga, Z. Giricz, G. Salinas, J. C. Gross, and L. C. Zelarayan, *Commun. Biol.* **6**(1), 79 (2023).
- ²³F. Provenzano, S. Nyberg, D. Giunti, C. Torazza, B. Parodi, T. Bonifacino, C. Usai, N. K. de Rosbo, M. Milanese, A. Uccelli, P. J. Shaw, L. Ferraiuolo, and G. Bonanno, *Cells* **11**(23), 3923 (2022).
- ²⁴A. von Eckardstein, B. G. Nordestgaard, A. T. Remaley, and A. L. Catapano, *Eur. Heart J.* **44**(16), 1394–1407 (2023).
- ²⁵O. N. Poteryaeva and I. F. Usynin, *Klin. Lab. Diagn.* **67**(7), 381–390 (2022).
- ²⁶E. Grao-Cruces, S. Lopez-Enriquez, M. E. Martin, and S. Montserrat-de la Paz, *Int. J. Biol. Macromol.* **195**, 117–123 (2022).
- ²⁷E. Grao-Cruces, L. M. Varela, M. E. Martin, B. Bermudez, and S. Montserrat-de la Paz, *Nutrients* **13**(3), 955 (2021).
- ²⁸M. G. Sorci-Thomas and M. J. Thomas, *Arterioscler. Thromb. Vasc. Biol.* **32**(11), 2561–2565 (2012).
- ²⁹M. Jansen and C. Contini, *PLoS One* **17**(7), e0272050 (2022).
- ³⁰G. Pichler, N. Amigo, M. Tellez-Plaza, M. A. Pardo-Cea, A. Dominguez-Lucas, V. G. Marrachelli, D. Monleon, J. C. Martin-Escudero, J. F. Ascaso, F. J. Chaves, R. Carmena, and J. Redon, *Int. J. Cardiol.* **264**, 172–178 (2018).
- ³¹M. R. Diffenderfer and E. J. Schaefer, *Curr. Opin. Lipidol.* **25**(3), 221–226 (2014).
- ³²H. C. Lee, W. C. Cheng, W. L. Ma, Y. H. Lin, S. J. Shin, and Y. H. Lin, *Sci. Rep.* **13**(1), 6575 (2023).
- ³³M. C. P. Roland, K. Godang, P. Aukrust, T. Henriksen, and T. Lekva, *Sci. Rep.* **11**(1), 6213 (2021).
- ³⁴I. Cruz-Bautista, R. Mehta, J. Cabiedes, C. García-Ulloa, L. E. Guillen-Pineda, P. Almeda-Valdés, D. Cuevas-Ramos, and C. A. Aguilar-Salinas, *Clin. Chim. Acta* **438**, 160–165 (2015).
- ³⁵Q. Wang, S. Li, L. Jiang, Y. Zhou, Z. Li, M. Shao, W. Li, and Y. Liu, *J. Lipid Res.* **51**(9), 2516–2526 (2010).
- ³⁶H. Zhang and D. Lyden, *Nat. Protoc.* **14**(4), 1027–1053 (2019).
- ³⁷Q. Zhang, D. K. Jeppesen, J. N. Higginbotham, R. Graves-Deal, V. Q. Trinh, M. A. Ramirez, Y. Sohn, A. C. Neininger, N. Taneja, E. T. McKinley, H. Niitsu, Z. Cao, R. Evans, S. E. Glass, K. C. Ray, W. H. Fissell, S. Hill, K. L. Rose, W. J. Huh, M. K. Washington, G. D. Ayers, D. T. Burnette, S. Sharma, L. H. Rome, J. L. Franklin, Y. A. Lee, Q. Liu, and R. J. Coffey, *Nat. Cell Biol.* **23**(12), 1240–1254 (2021).
- ³⁸N. Seo, J. Nakamura, T. Kaneda, H. Tateno, A. Shimoda, T. Ichiki, K. Furukawa, J. Hirabayashi, K. Akiyoshi, and H. Shiku, *J. Extracell. Vesicles* **11**(3), e12205 (2022).
- ³⁹H. K. Jackson, C. Mitoko, F. Linke, D. Macarthur, I. D. Kerr, and B. Coyle, *Cancers* **15**(9), 2601 (2023).
- ⁴⁰G. Dobrá, E. Gyukity-Sebestyén, M. Bükva, M. Harmati, V. Nagy, Z. Szabó, T. Pankotai, A. Klekner, and K. Buzás, *Cancers* **15**(3), 712 (2023).
- ⁴¹J. S. Redzic, A. A. Kendrick, K. Bahmed, K. D. Dahl, C. G. Pearson, W. A. Robinson, S. E. Robinson, M. W. Graner, and E. Z. Eisenmesser, *PLoS One* **8**(8), e71225 (2013).
- ⁴²S. Jayaraman, G. Cavigilio, and O. Gursky, *Biochem. J.* **442**(3), 703–712 (2012).
- ⁴³A. C. Rutledge, Q. Su, and K. Adeli, *Biochem. Cell Biol.* **88**(2), 251–267 (2010).
- ⁴⁴L. S. Kumpula, J. M. Kumpula, M. R. Taskinen, M. Jauhainen, K. Kaski, and M. Ala-Korpela, *Chem. Phys. Lipids* **155**(1), 57–62 (2008).
- ⁴⁵D. M. Yellon and S. M. Davidson, *Circ. Res.* **114**(2), 325–332 (2014).
- ⁴⁶E. Cocucci and J. Meldolesi, *Trends Cell Biol.* **25**(6), 364–372 (2015).
- ⁴⁷V. Sokolova, A. K. Ludwig, S. Hornung, O. Rotan, P. A. Horn, M. Epple, and B. Giebel, *Colloids Surf. B* **87**(1), 146–150 (2011).
- ⁴⁸G. Palmisano, S. S. Jensen, M. C. Le Bihan, J. Lainé, J. N. McGuire, F. Pociot, and M. R. Larsen, *Mol. Cell. Proteomics* **11**(8), 230–243 (2012).
- ⁴⁹I. H. Chen, L. Xue, C. C. Hsu, J. S. Paez, L. Pan, H. Andaluz, M. K. Wendt, A. B. Iliuk, J. K. Zhu, and W. A. Tao, *Proc. Natl. Acad. Sci. U.S.A.* **114**(12), 3175–3180 (2017).
- ⁵⁰A. Li, T. Zhang, M. Zheng, Y. Liu, and Z. Chen, *J. Hematol. Oncol.* **10**(1), 175 (2017).
- ⁵¹M. Xiong, Q. Zhang, W. Hu, C. Zhao, W. Lv, Y. Yi, Y. Wu, and M. Wu, *Front. Cell Dev. Biol.* **8**, 574223 (2020).
- ⁵²E. Gobin, K. Bagwell, J. Wagner, D. Mysona, S. Sandirasegarane, N. Smith, S. Bai, A. Sharma, R. Schleifer, and J. X. She, *BMC Cancer* **19**(1), 581 (2019).
- ⁵³M. Belhocine, T. Gernigon-Spychalowicz, M. P. Jacob, Y. Benazzoug, and J. M. Exbrayat, *Histol. Histopathol.* **25**(5), 619–636 (2010).
- ⁵⁴J. Hakulinen, L. Sankkila, N. Sugiyama, K. Lehti, and J. Keski-Oja, *J. Cell. Biochem.* **105**(5), 1211–1218 (2008).
- ⁵⁵D. K. Jeppesen, A. M. Fenix, J. L. Franklin, J. N. Higginbotham, Q. Zhang, L. J. Zimmerman, D. C. Liebler, J. Ping, Q. Liu, R. Evans, W. H. Fissell, J. G. Patton, L. H. Rome, D. T. Burnette, and R. J. Coffey, *Cell* **177**(2), 428–445.e18 (2019).
- ⁵⁶H. Zhang, D. Freitas, H. S. Kim, K. Fabijanic, Z. Li, H. Chen, M. T. Mark, H. Molina, A. B. Martin, L. Bojmar, J. Fang, S. Rampersaud, A. Hoshino, I. Matei, C. M. Kenific, M. Nakajima, A. P. Mutvei, P. Sansone, W. Buehring, H. Wang, J. P. Jimenez, L. Cohen-Gould, N. Paknejad, M. Brendel, K. Manova-Todorova, A. Magalhaes, J. A. Ferreira, H. Osorio, A. M. Silva, A. Massey, J. R. Cubillos-Ruiz, G. Galletti, P. Giannakakou, A. M. Cuervo, J. Blenis, R. Schwartz, M. S. Brady, H. Peinado, J. Bromberg, H. Matsui, C. A. Reis, and D. Lyden, *Nat. Cell Biol.* **20**(3), 332–343 (2018).
- ⁵⁷J. Choi, H. Y. Cho, J. Jeon, K. A. Kim, Y. D. Han, J. B. Ahn, I. Wortzel, D. Lyden, and H. S. Kim, *Front. Oncol.* **12**, 1067210 (2022).
- ⁵⁸R. Pirlög and G. A. Calin, *J. Clin. Invest.* **132**(14), e161454 (2022).
- ⁵⁹Z. Fong and W. L. Lee, *Future Med. Chem.* **14**(11), 827–845 (2022).
- ⁶⁰D. W. Hagey, M. Kordes, A. Gorgens, M. O. Mowoe, J. Z. Nordin, C. F. Moro, J. M. Lohr, and S. El Andaloussi, *J. Extracell. Vesicles* **10**(12), e12142 (2021).
- ⁶¹K. Allenson, J. Castillo, F. A. San Lucas, G. Scelo, D. U. Kim, V. Bernard, G. Davis, T. Kumar, M. Katz, M. J. Overman, L. Foretova, E. Fabianova, I. Holcatova, V. Janout, F. Meric-Bernstam, P. Gascoyne, I. Wistuba, G. Varadhachary, P. Brennan, S. Hanash, D. Li, A. Maitra, and H. Alvarez, *Ann. Oncol.* **28**(4), 741–747 (2017).
- ⁶²P. Peng, X. Wang, C. Qiu, W. Zheng, and H. Zhang, *Food Chem. Toxicol.* **180**, 114004 (2023).
- ⁶³C. Li, T. Qin, Y. Jin, J. Hu, F. Yuan, Y. Cao, and C. Duan, *J. Orthop. Transl.* **39**, 124–134 (2023).
- ⁶⁴Y. Zhuang, M. Cheng, M. Li, J. Cui, J. Huang, C. Zhang, J. Si, K. Lin, and H. Yu, *Acta Biomater.* **150**, 413–426 (2022).
- ⁶⁵R. Feng, Y. Yin, Y. Wei, Y. Li, L. Li, R. Zhu, X. Yu, Y. Liu, Y. Zhao, and Z. Liu, *Cancer Lett.* **562**, 216154 (2023).
- ⁶⁶C. G. Liu, J. Chen, R. M. W. Goh, Y. X. Liu, L. Wang, and Z. Ma, *Pharmacol. Res.* **191**, 106756 (2023).
- ⁶⁷M. Koni, T. Lopatina, C. Grange, A. Sarcinella, M. Cedrino, S. Bruno, F. Buffolo, S. Femmino, G. Camussi, and M. F. Brizzi, *Pharmacol. Res.* **195**, 106871 (2023).
- ⁶⁸E. Giovannetti and T. Li, *Cytokine Growth Factor Rev.* **73**, 1–2 (2023).
- ⁶⁹A. Al Hroud, M. P. Levesque, and R. Chahwan, *Front. Immunol.* **14**, 1176175 (2023).
- ⁷⁰E. Lázaro-Ibáñez, M. Neuvonen, M. Takatalo, U. Thanigai Arasu, C. Capasso, V. Cerullo, J. S. Rhim, K. Rilla, M. Yliperttula, and P. R. Siljander, *J. Extracell. Vesicles* **6**(1), 1354645 (2017).
- ⁷¹D. Garnier, N. Magnus, B. Meehan, T. Kislinger, and J. Rak, *Exp. Cell Res.* **319**(17), 2747–2757 (2013).
- ⁷²J. He, H. Li, J. Mai, Y. Ke, C. Zhai, J. J. Li, L. Jiang, G. Shen, and X. Ding, *J. Extracell. Vesicles* **12**(9), e12364 (2023).
- ⁷³C. Zhai, J. Long, J. He, Y. Zheng, B. Wang, J. Xu, Y. Yang, L. Jiang, H. Yu, and X. Ding, *ACS Nano* **17**(17), 16656–16667 (2023).

26 May 2025 19:54:44

- ⁷⁴A. Giovanazzi, M. J. C. van Herwijnen, M. Kleinjan, G. N. van der Meulen, and M. H. M. Wauben, *Sci. Rep.* **13**(1), 8758 (2023).
- ⁷⁵E. Manouchehri Douabi, C. Fredolini, R. Gallini, L. Löf, Q. Shen, R. Ikebuchi, L. Dubois, A. Azimi, O. Loudig, S. Gabrielsson, U. Landegren, A. Larsson, J. Bergquist, and M. Kamali-Moghaddam, *Commun. Biol.* **5**(1), 1402 (2022).
- ⁷⁶J. Burrello, M. Tetti, V. Forestiero, V. Biemmi, S. Bolis, M. A. C. Pomatto, M. Amongero, D. Di Silvestre, P. Mauri, G. Vassalli, G. Camussi, T. A. Williams, P. Mulaturo, L. Barile, and S. Monticone, *Hypertension* **78**(3), 726–737 (2021).
- ⁷⁷S. Cavallaro, J. Horak, P. Hägg, D. Gupta, C. Stiller, S. S. Sahu, A. Görgens, H. K. Gatty, K. Viktorsson, S. El Andaloussi, R. Lewensohn, A. E. Karlström, J. Linnros, and A. Dev, *ACS Sens.* **4**(5), 1399–1408 (2019).
- ⁷⁸A. Vandergriff, K. Huang, D. Shen, S. Hu, M. T. Hensley, T. G. Caranasos, L. Qian, and K. Cheng, *Theranostics* **8**(7), 1869–1878 (2018).
- ⁷⁹T. J. Antes, R. C. Middleton, K. M. Luther, T. Ijichi, K. A. Peck, W. J. Liu, J. Valle, A. K. Echavez, and E. Marban, *J. Nanobiotechnol.* **16**(1), 61 (2018).
- ⁸⁰A. Bryja, L. Zadka, M. Farzaneh, M. Zehtabi, M. Ghasemian, M. Dyszkiewicz-Konwinska, P. Mozdziak, M. Zabel, M. Podhorska-Okolow, P. Dziegieł, H. Piotrowska-Kempisty, and B. Kempisty, *Life Sci.* **332**, 122126 (2023).
- ⁸¹J. Li, Y. Zhang, P. Y. Dong, G. M. Yang, and S. Gurunathan, *Biomed. Pharmacother.* **165**, 115087 (2023).
- ⁸²B. F. Hettich, J. J. Bader, and J. C. Leroux, *Adv. Healthcare Mater.* **11**(5), e2100047 (2022).
- ⁸³Y. Zhang, G. Kim, Y. Zhu, C. Wang, R. Zhu, X. Lu, H. C. Chang, and Y. Wang, *ACS Nano* **17**(11), 10191–10205 (2023).
- ⁸⁴S. T. Chuang, Y. S. Shon, and V. Narayanaswami, *Int. J. Nanomed.* **12**, 8495–8510 (2017).
- ⁸⁵M. Krieger, L. C. Smith, R. G. Anderson, J. L. Goldstein, Y. J. Kao, H. J. Pownall, A. M. Gotto, Jr., and M. S. Brown, *J. Supramol. Struct.* **10**(4), 467–478 (1979).
- ⁸⁶G. Kharmate, E. Hosseini-Beheshti, J. Caradec, M. Y. Chin, and E. S. Tomlinson Guns, *PLoS One* **11**(5), e0154967 (2016).
- ⁸⁷Y. Tang, P. Zhang, Y. Wang, J. Wang, M. Su, Y. Wang, L. Zhou, J. Zhou, W. Xiong, Z. Zeng, Y. Zhou, S. Nie, and Q. Liao, *Front. Immunol.* **11**, 604 (2020).
- ⁸⁸G. Chen, A. C. Huang, W. Zhang, G. Zhang, M. Wu, W. Xu, Z. Yu, J. Yang, B. Wang, H. Sun, H. Xia, Q. Man, W. Zhong, L. F. Antelo, B. Wu, X. Xiong, X. Liu, L. Guan, T. Li, S. Liu, R. Yang, Y. Lu, L. Dong, S. McGettigan, R. Somasundaram, R. Radhakrishnan, G. Mills, Y. Lu, J. Kim, Y. H. Chen, H. Dong, Y. Zhao, G. C. Karakousis, T. C. Mitchell, L. M. Schuchter, M. Herlyn, E. J. Wherry, X. Xu, and W. Guo, *Nature* **560**(7718), 382–386 (2018).
- ⁸⁹V. Ciravolo, V. Huber, G. C. Ghedini, E. Venturelli, F. Bianchi, M. Campiglio, D. Morelli, A. Villa, P. Della Mina, S. Menard, P. Filipazzi, L. Rivoltini, E. Tagliabue, and S. M. Pupa, *J. Cell. Physiol.* **227**(2), 658–667 (2012).
- ⁹⁰C. Shibata, M. Otsuka, T. Seimiya, T. Kishikawa, K. Ishigaki, and M. Fujishiro, *Clin. Transl. Med.* **12**(11), e1089 (2022).
- ⁹¹S. Kaur, F. Livak, G. Daaboul, L. Anderson, and D. D. Roberts, *J. Extracell. Vesicles* **11**(9), e12265 (2022).
- ⁹²T. B. McKay, A. E. K. Hutcheon, and J. D. Zieske, *Eye* **34**(2), 271–278 (2020).
- ⁹³R. M. DeRita, A. Sayeed, V. Garcia, S. R. Krishn, C. D. Shields, S. Sarker, A. Friedman, P. McCue, S. K. Molugu, U. Rodeck, A. P. Dicker, and L. R. Languino, *iScience* **14**, 199–209 (2019).
- ⁹⁴M. P. Bebelman, C. Crudden, D. M. Pegtel, and M. J. Smit, *Trends Pharmacol. Sci.* **41**(9), 627–640 (2020).
- ⁹⁵R. M. DeRita, B. Zerlanko, A. Singh, H. Lu, R. V. Iozzo, J. L. Benovic, and L. R. Languino, *J. Cell. Biochem.* **118**(1), 66–73 (2017).
- ⁹⁶G. Deep, A. Jain, A. Kumar, C. Agarwal, S. Kim, W. M. Leevy, and R. Agarwal, *Mol. Carcinog.* **59**(3), 323–332 (2020).
- ⁹⁷Z. Latifi, A. Fattahai, A. Ranjbaran, H. R. Nejabati, and K. Imakawa, *J. Cell. Physiol.* **233**(6), 4530–4545 (2018).
- ⁹⁸N. Maniya, S. Kumar, J. L. Franklin, J. N. Higginbotham, A. M. Scott, H. K. Gan, R. J. Coffey, S. Senapati, and H.-C. Chang, *Commun. Biol.* **7**(1), 677 (2024).
- ⁹⁹G. Awanis, S. Banerjee, R. Johnson, S. Raveenthiraraj, A. Elmeliig, D. Warren, J. Gavrilovic, and A. Sobolewski, *Life Sci. Alliance* **6**(10), e202301953 (2023).
- ¹⁰⁰S. L. Andrews, M. Ghaderi-Najafabadi, P. Gong, N. Shamkhi, L. Carlton, C. Schofield, T. Kessler, N. J. Samani, T. R. Webb, and G. E. Morris, *Biochim. Biophys. Acta Mol. Cell Res.* **1870**(6), 119479 (2023).
- ¹⁰¹F. Draicchio, V. Behrends, N. A. Tillin, N. M. Hurren, L. Sylow, and R. Mackenzie, *J. Physiol.* **600**(20), 4393–4408 (2022).
- ¹⁰²J. Zhou, A. Wang, T. Cai, Y. Li, W. Du, Y. Zhang, R. Zhang, W. Zhang, J. Zhu, Y. Zeng, J. A. Huang, and Z. Liu, *Cell Death Dis.* **13**(5), 486 (2022).
- ¹⁰³A. R. Shen, X. Zhong, T. T. Tang, C. Wang, J. Jing, B. C. Liu, and L. L. Lv, *Front. Physiol.* **11**, 627800 (2021).
- ¹⁰⁴K. Jiang, C. Dong, Z. Yin, R. Li, J. Mao, C. Wang, J. Zhang, Z. Gao, R. Liang, Q. Wang, and L. Wang, *Cell Death Dis.* **11**(11), 972 (2020).
- ¹⁰⁵Y. Yue, C. Wang, C. Benedict, G. Huang, M. Truongcao, R. Roy, M. Cimini, V. N. S. Garikipati, Z. Cheng, W. J. Koch, and R. Kishore, *Circ. Res.* **126**(3), 315–329 (2020).
- ¹⁰⁶A. Singh, C. Fedele, H. Lu, M. T. Nevalainen, J. H. Keen, and L. R. Languino, *Mol. Cancer Res.* **14**(11), 1136–1146 (2016).
- ¹⁰⁷J. Skog, T. Würdinger, S. Van Rijn, D. H. Meijer, L. Gainche, W. T. Curry, Jr., B. S. Carter, A. M. Krichevsky, and X. O. Breakfield, *Nat. Cell Biol.* **10**(12), 1470–1476 (2008).
- ¹⁰⁸J. M. Figueiroa, J. Skog, J. Akers, H. Li, R. Komotar, R. Jensen, F. Ringel, I. Yang, S. Kalkanis, R. Thompson, and L. LoGuidice, *Neuro-Oncology* **19**(11), 1494–1502 (2017).
- ¹⁰⁹M. Rosenblat, R. Karry, and M. Aviram, *Atherosclerosis* **187**(1), 74.e1–74.e10 (2006).
- ¹¹⁰S. Kumar, N. Maniya, C. Wang, S. Senapati, and H. C. Chang, *Nat. Commun.* **14**(1), 557 (2023).
- ¹¹¹S. Saman, W. Kim, M. Raya, Y. Visnick, S. Miro, S. Saman, B. Jackson, A. C. McKee, V. E. Alvarez, N. C. Lee, and G. F. Hall, *J. Biol. Chem.* **287**(6), 3842–3849 (2012).
- ¹¹²A. Montagne, A. M. Nikolakopoulou, M. T. Huusonen, A. P. Sagare, E. J. Lawson, D. Lazic, S. V. Rege, A. Grond, E. Zuniga, S. R. Barnes, J. Prince, M. Sagare, C. J. Hsu, M. J. LaDu, R. E. Jacobs, and B. V. Zlokovic, *Nat. Aging* **1**(6), 506–520 (2021).
- ¹¹³J. L. Robinson, E. B. Lee, S. X. Xie, L. Rennert, E. Suh, C. Bredenberg, C. Caswell, V. M. Van Deerlin, N. Yan, A. Yousef, H. I. Hurtig, A. Siderowf, M. Grossman, C. T. McMillan, B. Miller, J. E. Duda, D. J. Irwin, D. Wolk, L. Elman, L. McCluskey, A. Chen-Plotkin, D. Weintraub, S. E. Arnold, J. Brettschneider, V. M. Lee, and J. Q. Trojanowski, *Brain* **141**(7), 2181–2193 (2018).
- ¹¹⁴F. A. W. Coumans, A. R. Brisson, E. I. Buzas, F. Dignat-George, E. E. E. Drees, S. El-Andaloussi, C. Emanueli, A. Gasecka, A. Hendrix, A. F. Hill, R. Lacroix, Y. Lee, T. G. van Leeuwen, N. Mackman, I. Mager, J. P. Nolan, E. van der Pol, D. M. Pegtel, S. Sahoo, P. R. M. Siljander, G. Sturk, O. de Wever, and R. Nieuwland, *Circ. Res.* **120**(10), 1632–1648 (2017).
- ¹¹⁵M. Wu, C. Chen, Z. Wang, H. Bachman, Y. Ouyang, P. H. Huang, Y. Sadovsky, and T. J. Huang, *Lab Chip* **19**(7), 1174–1182 (2019).
- ¹¹⁶L. Cheng, R. A. Sharples, B. J. Scicluna, and A. F. Hill, *J. Extracell. Vesicles* **3**, 23743 (2014).
- ¹¹⁷H. Sharma, V. Yadav, C. D'Souza-Schorey, D. B. Go, S. Senapati, and H. C. Chang, *ACS Nano* **17**(10), 9388–9404 (2023).
- ¹¹⁸B. W. Sodar, A. Kittel, K. Paloczi, K. V. Vukman, X. Osteikoetxea, K. Szabo-Taylor, A. Nemeth, B. Sperlagh, T. Baranyai, Z. Giricz, Z. Wiener, L. Turiak, L. Drahos, E. Pallinger, K. Vekey, P. Ferdinand, A. Falus, and E. I. Buzas, *Sci. Rep.* **6**, 24316 (2016).
- ¹¹⁹M. Mustapic, E. Eitan, J. K. Werner, Jr., S. T. Berkowitz, M. P. Lazaropoulos, J. Tran, E. J. Goetzl, and D. Kapogiannis, *Front. Neurosci.* **11**, 278 (2017).
- ¹²⁰L. A. Newman, Z. Useckaitė, J. Johnson, M. J. Sorich, A. M. Hopkins, and A. Rowland, *Biomedicines* **10**(1), 195 (2022).
- ¹²¹D. Li, W. Lai, D. Fan, and Q. Fang, *Am. J. Physiol. Cell Physiol.* **321**(5), C779–C797 (2021).

- ¹²²Y. T. Wang, T. Shi, S. Srivastava, J. Kagan, T. Liu, and K. D. Rodland, *Cancers (Basel)* **12**(9), 2335 (2020).
- ¹²³T. An, S. Qin, D. Sun, Y. Huang, Y. Hu, S. Li, H. Zhang, B. Li, B. Situ, L. Lie, Y. Wu, and L. Zheng, *Proteomics* **19**(12), e1800160 (2019).
- ¹²⁴C. J. Beckham, J. Olsen, P. N. Yin, C. H. Wu, H. J. Ting, F. K. Hagen, E. Scosyrev, E. M. Messing, and Y. F. Lee, *J. Urol.* **192**(2), 583–592 (2014).
- ¹²⁵G. A. Francis, A. J. Mendez, E. L. Bierman, and J. W. Heinecke, *Proc. Natl. Acad. Sci. U.S.A.* **90**(14), 6631–6635 (1993).
- ¹²⁶F. Natella, M. Nardini, F. Ursini, and C. Scaccini, *Free Radical Res.* **29**(5), 427–434 (1998).
- ¹²⁷P. D. Thomas and M. J. Poznansky, *Anal. Biochem.* **188**(1), 228–232 (1990).
- ¹²⁸D. Pedone, M. Moglianetti, M. Lettieri, G. Marrazza, and P. P. Pompa, *Anal. Chem.* **92**(13), 8660–8664 (2020).
- ¹²⁹L. Li, S. Wang, J. Xue, Y. Lin, L. Su, C. Xue, C. Mao, N. Cai, Y. Tian, S. Zhu, L. Wu, and X. Yan, *Anal. Chem.* **95**(6), 3423–3433 (2023).
- ¹³⁰R. Lees, R. Tempest, A. Law, D. Aubert, O. G. Davies, S. Williams, N. Peake, and B. Peacock, *J. Vis. Exp.* **26**(185), e64020 (2022).
- ¹³¹C. Chen, N. Cai, Q. Niu, Y. Tian, Y. Hu, and X. Yan, *J. Extracell. Vesicles* **12**(8), e12351 (2023).
- ¹³²J. M. J. Price, Y. Hisada, J. Hazeldine, V. Bae-Jump, T. Luther, N. Mackman, and P. Harrison, *Res. Pract. Thromb. Haemostasis* **7**(4), 100177 (2023).
- ¹³³K. Breitwieser, L. F. Koch, T. Tertel, E. Proestler, L. D. Burgers, C. Lipps, J. Adjaye, R. Furst, B. Giebel, and M. J. Saul, *Int. J. Mol. Sci.* **23**(15), 8544 (2022).
- ¹³⁴L. C. Zanetti-Domingues, C. J. Tynan, D. J. Rolfe, D. T. Clarke, and M. Martin-Fernandez, *PLoS One* **8**(9), e74200 (2013).
- ¹³⁵R. Tapec, X. J. Zhao, and W. Tan, *J. Nanosci. Nanotechnol.* **2**(3–4), 405–409 (2002).
- ¹³⁶L. A. Andronico, S. R. Jung, B. S. Fujimoto, and D. T. Chiu, *Anal. Chem.* **95**(28), 10492–10497 (2023).
- ¹³⁷B. C. Ferrari and P. L. Bergquist, *Cytometry, Part A* **71A**(4), 265–271 (2007).
- ¹³⁸K. P. McCarthy, D. B. Go, S. Senapati, and H. C. Chang, *Lab Chip* **23**(2), 285–294 (2023).
- ¹³⁹S. Sensale, Z. Ramshani, S. Senapati, and H. C. Chang, *J. Phys. Chem. B* **125**(7), 1906–1915 (2021).
- ¹⁴⁰Z. Ramshani, C. Zhang, K. Richards, L. Chen, G. Xu, B. L. Stiles, R. Hill, S. Senapati, D. B. Go, and H. C. Chang, *Commun. Biol.* **2**, 189 (2019).
- ¹⁴¹D. Taller, K. Richards, Z. Slouka, S. Senapati, R. Hill, D. B. Go, and H. C. Chang, *Lab Chip* **15**(7), 1656–1666 (2015).
- ¹⁴²Z. Slouka, S. Senapati, and H. C. Chang, *Annu. Rev. Anal. Chem. (Palo Alto Calif.)* **7**, 317–335 (2014).
- ¹⁴³S. Senapati, Z. Slouka, S. S. Shah, S. K. Behura, Z. Shi, M. S. Stack, D. W. Severson, and H. C. Chang, *Biosens. Bioelectron.* **60**, 92–100 (2014).
- ¹⁴⁴Z. Ramshani, F. Fan, A. Wei, M. Romanello-Giroud-Joaquim, C. H. Gil, M. George, M. C. Yoder, D. Hanjaya-Putra, S. Senapati, and H. C. Chang, *Talanta* **225**, 122021 (2021).
- ¹⁴⁵G. N. Fu, Y. Z. He, L. Wang, and X. K. Wang, *Anal. Sci.* **22**(6), 883–887 (2006).
- ¹⁴⁶J. W. Lewis, S. Jager, and D. S. Kliger, *Photochem. Photobiol.* **66**(6), 741–746 (1997).
- ¹⁴⁷F. W. Teale and G. Weber, *Biochem. J.* **65**(3), 476–482 (1957).
- ¹⁴⁸I. Iosub, M. Giurgenica, N. Iftimie, and A. Meghea, *Mol. Cryst. Liq. Cryst.* **448**(1), 39/[641]–49/[651] (2006).
- ¹⁴⁹E. Stern, R. Wagner, F. J. Sigworth, R. Breaker, T. M. Fahmy, and M. A. Reed, *Nano Lett.* **7**(11), 3405–3409 (2007).
- ¹⁵⁰V. Kesler, B. Murmann, and H. T. Soh, *ACS Nano* **14**(12), 16194–16201 (2020).
- ¹⁵¹C. Zhang, G. Sun, S. Senapati, and H. C. Chang, *Lab Chip* **19**(22), 3853–3861 (2019).
- ¹⁵²G. Sun, S. Senapati, and H. C. Chang, *Lab Chip* **16**(7), 1171–1177 (2016).
- ¹⁵³H.-C. Chang, G. Yossifon, and E. A. Demekhin, *Annu. Rev. Fluid Mech.* **44**(1), 401–426 (2012).
- ¹⁵⁴J. N. Chuang, P. Y. Diao, W. S. Huang, L. F. Huang, S. Senapati, H. C. Chang, and Y. M. Sun, *ACS Appl. Mater. Interfaces* **12**(49), 54459–54472 (2020).
- ¹⁵⁵C. M. Yang, J. C. Yu, P. Y. Chu, C. H. Hsieh, and M. H. Wu, *Biosensors* **12**(9), 755 (2022).
- ¹⁵⁶N. H. Thi Tran, T. B. Phan, T. T. Nguyen, and H. Ju, *Biosens. Bioelectron.* **176**, 112900 (2021).
- ¹⁵⁷J. Su, W. Liu, S. Chen, W. Deng, Y. Dou, Z. Zhao, J. Li, Z. Li, H. Yin, X. Ding, and S. Song, *ACS Sens.* **5**(12), 3979–3987 (2020).
- ¹⁵⁸Z. Li, Y. Liu, X. Chen, H. Cao, H. Shen, L. Mou, X. Deng, X. Jiang, and Y. Cong, *Biosens. Bioelectron.* **166**, 112444 (2020).
- ¹⁵⁹J. Qian, N. Xu, X. Zhou, K. Shi, Q. Du, X. Yin, and Z. Zhao, *Int. J. Nanomed.* **14**, 7431–7446 (2019).
- ¹⁶⁰R. Zhai, G. Chen, G. Liu, X. Huang, X. Xu, L. Li, Y. Zhang, D. Xu, and A. M. Abd El-Aty, *Foods* **12**(1), 196 (2023).
- ¹⁶¹M. K. Rauf, D. Jordan, H. Auer, J. M. Warnecke, B. Lepenies, and C. Strube, *Parasitology* **148**(3), 333–340 (2021).
- ¹⁶²S. Deininger and N. Wellinghausen, *GMS Infect. Dis.* **7**, Doc01 (2019).
- ¹⁶³A. Frutiger, A. Tanno, S. Hwu, R. F. Tiefenauer, J. Voros, and N. Nakatsuka, *Chem. Rev.* **121**(13), 8095–8160 (2021).
- ¹⁶⁴D. Li, C. Wang, G. Sun, S. Senapati, and H. C. Chang, *Biosens. Bioelectron.* **97**, 143–149 (2017).
- ¹⁶⁵J. T. Melchior, S. E. Street, T. Vaisar, R. Hart, J. Jerome, Z. Kuklenyik, N. Clouet-Foraison, C. Thorneck, S. Bedi, A. S. Shah, J. P. Segrest, J. W. Heinecke, and W. S. Davidson, *J. Lipid Res.* **62**, 100099 (2021).
- ¹⁶⁶A. R. Brisson, S. Tan, R. Linares, C. Gounou, and N. Arraud, *Platelets* **28**(3), 263–271 (2017).
- ¹⁶⁷S. A. Melo, L. B. Luecke, C. Kahlert, A. F. Fernandez, S. T. Gammon, J. Kaye, V. S. LeBleu, E. A. Mittendorf, J. Weitz, N. Rahbari, C. Reissfelder, C. Pilarsky, M. F. Fraga, D. Piwnica-Worms, and R. Kalluri, *Nature* **523**(7559), 177–182 (2015).
- ¹⁶⁸X. Meng, P. Kukura, and S. Faez, *Nanoscale* **13**(29), 12687–12696 (2021).
- ¹⁶⁹H.-C. Chang and L. Yeo, *Electrokinetically Driven Microfluidics and Nanofluidics* (Cambridge University Press, 2010).

26 May 2025 19:54:44